JOURNAL OF GUIDANCE, CONTROL, AND DYNAMICS
Vol. 30, No. 4, July–August 2007

# Adaptive Disturbance Rejection Controller for Visual Tracking of a Maneuvering Target

Vahram Stepanyan* and Naira Hovakimyan†
*Virginia Polytechnic Institute and State University, Blacksburg, Virginia 24061*

DOI: 10.2514/1.25034

**This paper presents an adaptive disturbance rejection control architecture for a flying vehicle to track a maneuvering target using a monocular camera as a visual sensor. Viewing the target's velocity as a time-varying disturbance, the change in magnitude of which has a bounded integral, a guidance law is derived that guarantees asymptotic tracking of the target in the presence of measurement noise and an intelligent excitation signal in the reference input. Implementation of the guidance law is done via conventional adaptive block backstepping. Simulations illustrate the benefits of the method.**

## I. Introduction

ONE of the most challenging problems in the unmanned air vehicle (UAV) or micro air vehicle (MAV) development is the design of a vision-based guidance system that is capable of tracking a maneuvering target using only visual information. The main difference between the problem of visual tracking and the standard tracking problems is the way the feedback signal is measured. Visual tracking is done via imaging sensors, which involves a projection of a three-dimensional object onto a two-dimensional plane, consequently rendering the range between the two flying objects unobservable. In addition, we note that the range information has to be extracted via computer vision algorithms before being used in the control loop. Consequently, from the classical control theoretical point of view, one can formulate this as a disturbance rejection/attenuation problem in the presence of a highly uncertain time-varying disturbance associated with unpredictable target dynamics.

The target tracking problem (without the visual sensors) is a relatively old one, and there is extensive literature in this field, addressing the topic from various perspectives. The fundamental issue in this problem is the lack of complete information about the target's dynamics. We note that, dependent upon the choice of the coordinate system, either the system dynamics or the measurement are nonlinear. For example, in Cartesian coordinates the dynamic equations are linear, but the observation model is nonlinear [1,2], whereas in the spherical coordinate system the observation model is linear at the expense of a highly nonlinear dynamic model [3–5]. In most cases, the extended Kalman filter (EKF) or modified EKF has been the main tool for extracting necessary information about the target dynamics. Modifications of EKF include adaptive EKFs [6], multiple model adaptive estimators which identify the target maneuver based on some prestored models [7,8], iterated extended Kalman filter (IEKF) which has an improved performance and a better accuracy [9], or two-step optimal estimators that divide the estimation into a "linear first step" using the standard Kalman filter and a "nonlinear second step" that treats states estimated via the Kalman filter as measurements for the nonlinear least-squares fit [1]. Convergence properties for EKF have been proven in [10] for linear deterministic models with unknown coefficients in a discrete-time setting. Because with visual sensors the state-space representation for the system is nonlinear either in the states (spherical coordinate system [3–5]) or in the measurement equation (Cartesian coordinate system [1,2]), the results from [10] cannot be used without additional asymptotic analysis.

It has been observed that the relative range is unobservable from the bearing-only measurement (for example, see [3]), and a special type of ownship maneuvers is required to overcome this issue. Another way is to look for additional information that can be extracted from the image processing algorithm. Betser et al. [11] have used the maximum angle subtended by the target in the image plane. This angular measurement relates the unobservable range to the unknown target's geometric size, rendering the relative range observable if the target's geometry is known. Unfortunately, this is generally not the case, and special types of maneuvers are required from the follower to overcome the unobservability even if the target maintains constant velocity. These maneuvers are called *excitation* of the reference signal in the adaptive control framework. In [12], the notion of intelligent excitation has been introduced to replace the stringent requirement for the persistent excitation, which is the common tool in adaptive control for achieving parameter convergence. The amplitude of this excitation is modulated dependent upon the tracking error, and therefore guarantees simultaneous parameter convergence and reference command tracking.

In UAV applications, vision-based algorithms have been used for path planning and the vehicle's state estimation in unknown environments. The authors in [13–15] have used a combination of methods from the statistical learning theory [16] and structure-from-motion (SFM) algorithms to do map/image reconstruction and estimation of the vehicle's states in the absence of any tracking tasks. In [14], an implicit extended Kalman filter and epipolar constraint are used for the state estimation of the UAV. A brief overview of feature-point tracking and SFM algorithms, which can be applied to the problem of aerial vehicles' state estimation, can be found in [13]. In the visual target tracking problems, existing results mainly consider target motions with constant velocity [3,11] or model the target's acceleration as a zero-mean Gaussian process [17]. Adaptive output feedback control framework has been explored in [17–19] under a certain set of assumptions about the target dynamics. The derived controller guarantees tracking with ultimately bounded error, but this bound cannot be quantified.

In this paper, we consider the tracking problem of a maneuvering target using only visual information about the target. The target's velocity is viewed as a time-varying disturbance that can be decomposed into sum of a constant term and a time-varying term that has bounded integral of its 2-norm over time. Scaling the relative states by the unknown target size reformulates the problem into a framework with an information deficit in the reference commands.

Presented as Paper 6000 at the AIAA Guidance, Navigation, and Control Conference and Exhibit, San Francisco, California, 15–18 August 2005; received 8 May 2006; revision received 28 November 2006; accepted for publication 14 January 2007. 

*Graduate Research Assistant, Department of Aerospace and Ocean Engineering. Student Member AIAA.

†Associate Professor, Department of Aerospace and Ocean Engineering. Senior Member AIAA.

Additionally, the problem is complicated by the presence of unknown time-varying disturbances associated with the target's velocity and the measurement noise. The outer-loop control uses the adaptive synthesis approach developed in [20] to derive a guidance law that rejects the time-varying disturbances and, as a result, guarantees asymptotic tracking of estimated reference commands. Introducing an intelligent excitation signal [12] in the reference input guarantees simultaneous convergence of the estimated reference commands to the true ones and convergence of the true tracking error to zero. The inner-loop control for the implementation of the guidance law on a full nonlinear model of an aircraft is performed using adaptive backstepping with radial basis function (RBF) neural networks for the approximation of modeling uncertainties and atmospheric turbulence.

The rest of the paper is organized as follows. First, we give the problem formulation and the state-space representation. Then, the adaptive disturbance rejection guidance law is presented, and the relevant parameter convergence is analyzed. Next, the approach is extended to the case of noisy measurements. Finally, adaptive backstepping is presented for derivation of the inner-loop controllers. Simulation results demonstrate the performance of the guidance law.

Throughout the paper, bold symbols denote vector quantities.

## II. Problem Formulation

In a kinematic setting, the equation of motion for the flying target is given by

$$\dot{\boldsymbol{R}}_T(t) = \boldsymbol{V}_T(t), \qquad \boldsymbol{R}_T(0) = \boldsymbol{R}_{T_0} \tag{1}$$

where $\boldsymbol{R}_T(t) = \begin{bmatrix} x_T(t) & y_T(t) & z_T(t) \end{bmatrix}^\top$ and $\boldsymbol{V}_T(t) = \begin{bmatrix} V_{T_x}(t) & V_{T_y}(t) & V_{T_z}(t) \end{bmatrix}^\top$ are, respectively, the position and velocity vectors of the target's center of gravity in some inertial frame $F_E = (x_E, y_E, z_E)$ (Fig. 1). An autonomous aerial vehicle, called in the sequel a follower, is described by the equation

$$\dot{\boldsymbol{R}}_F(t) = \boldsymbol{V}_F(t), \qquad \boldsymbol{R}_F(0) = \boldsymbol{R}_{F_0} \tag{2}$$

where $\boldsymbol{R}_F(t) = \begin{bmatrix} x_F(t) & y_F(t) & z_F(t) \end{bmatrix}^\top$ and $\boldsymbol{V}_F(t) = \begin{bmatrix} V_{F_x}(t) & V_{F_y}(t) & V_{F_z}(t) \end{bmatrix}^\top$ are, respectively, the follower's position and velocity vectors in the same inertial frame $F_E$ (Fig. 1).

We assume that the follower can measure its own states and can get visual information about the target via a single camera that is fixed on the follower with its optical axis parallel to the follower's longitudinal $x_B$ axis of the body frame $F_B = (x_B, y_B, z_B)$, and its optical center fixed at the follower's center of gravity. Then the body frame can be chosen coincident with the camera frame (Fig. 1). It is assumed that the image processing algorithm associated with the camera provides three measurements in real time. These are the pixel coordinates of the image centroid $(y_I, z_I)$ in the image plane and the image length $b_I$ in pixels (Fig. 2). Assuming that the camera focal length $l$ is known, the bearing angle $\lambda$, the elevation angle $\vartheta$ can be expressed via the measurements through the geometric relationships (Fig. 1):

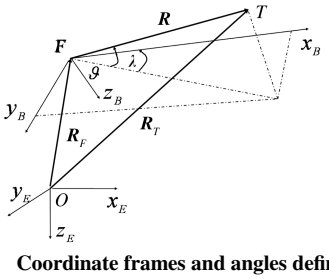


**Fig. 1 Coordinate frames and angles definition.**

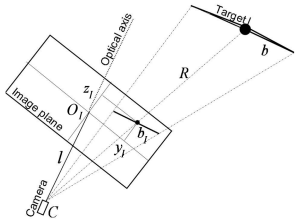


**Fig. 2 Camera frame and measurements.**

$$\tan\lambda = \frac{y_I}{l}, \qquad \tan\vartheta = \frac{z_I}{\sqrt{l^2 + y_I^2}} \tag{3}$$

The target's relative position with respect to the follower is given by the inertial vector (see Fig. 1)

$$\boldsymbol{R} = \boldsymbol{R}_T - \boldsymbol{R}_F \tag{4}$$

Hence, the relative dynamics in the inertial frame is given by the equation

$$\dot{\boldsymbol{R}}(t) = \boldsymbol{V}_T(t) - \boldsymbol{V}_F(t), \qquad \boldsymbol{R}(0) = \boldsymbol{R}_0 \tag{5}$$

where the initial conditions are given by $\boldsymbol{R}_0 = \boldsymbol{R}_{T_0} - \boldsymbol{R}_{F_0}$.

We notice that the relative position $\boldsymbol{R}$ and the relative velocity $\boldsymbol{V}$ are not measurable, because no information about the target's motion is assumed except for the visual measurements $y_I, z_I, b_I$. However, the relative position $\boldsymbol{R}$ can be related to the measurements $y_I, z_I, b_I$ as follows. From the geometric considerations, we observe that the relative range $R = \|\boldsymbol{R}\|$ can be expressed as

$$R = \frac{b_T}{b_I}\sqrt{l^2 + y_I^2 + z_I^2} \triangleq b_T a_I \tag{6}$$

where $b_T > 0$ is the maximum apparent size of the target that is assumed to be a constant. Therefore, the relative position can be expressed in the follower's body frame as follows

$$\boldsymbol{R}^B = R\boldsymbol{T}_{IB} = b_T a_I \boldsymbol{T}_{IB} \tag{7}$$

where the vector $\boldsymbol{T}_{IB}$ is defined as

$$\boldsymbol{T}_{IB} = \begin{bmatrix} \cos\vartheta\cos\lambda \\ \cos\vartheta\sin\lambda \\ -\sin\vartheta \end{bmatrix} \tag{8}$$

Using the coordinate transformation matrix $L_{B/E}$ from the inertial frame $F_E$ to the follower's body frame $F_B$

$$L_{B/E} = \begin{bmatrix} c\theta s\psi & c\theta c\psi & -s\theta \\ s\phi s\theta c\psi - c\phi s\psi & s\phi s\theta s\psi + c\phi c\psi & s\phi c\theta \\ c\phi s\theta c\psi + s\phi s\psi & c\phi s\theta s\psi - s\phi c\psi & c\phi c\theta \end{bmatrix}$$

where for the sake of brevity we use $s$ for sin function and $c$ for cos function, and $\phi$, $\theta$, $\psi$ are the Euler angles associated with the frame $F_B$ [21] (p. 313), the inertial relative position vector $\boldsymbol{R}$ can be written as

$$\boldsymbol{R} = L_{B/E}^\top \boldsymbol{R}^B = b_T a_I L_{B/E}^\top \boldsymbol{T}_{IB} \tag{9}$$

In this form the relative position is computable up to the unknown scaling factor $b_T$. Therefore, we introduce the scaled relative position vector $\boldsymbol{r}(t) = \boldsymbol{R}(t)/b_T$, the dynamics of which are written as

$$\dot{\boldsymbol{r}}(t) = \frac{1}{b_T}[\boldsymbol{V}_T(t) - \boldsymbol{V}_F(t)], \qquad \boldsymbol{r}(0) = \boldsymbol{r}_0 \tag{10}$$

where $\boldsymbol{r}_0 = \boldsymbol{R}_0/b_T$. The vector $\boldsymbol{r}$ is related to the visual measurements via the following algebraic equation

$$\boldsymbol{r} = a_I L_{B/E}^\top \boldsymbol{T}_{IB} \tag{11}$$

and hence is available for feedback. However, the system (10) still involves the unknown velocity $\boldsymbol{V}_T(t)$. In addition, it depends upon the unknown constant parameter $b_T$.

The follower's objective is to maintain a desired relative position with respect to the target, which can be given either in the inertial frame $F_E$ in the form of the vector command $\boldsymbol{R}_{\text{com}}(t)$ or in the follower's body frame in the form of the relative range command $R_{\text{com}}(t)$, in addition to the bearing and the elevation commands $\lambda_{\text{com}}(t)$ and $\vartheta_{\text{com}}(t)$, respectively. In the latter case the reference commands need to be translated to the inertial frame as follows

$$\boldsymbol{R}_{\text{com}}(t) = R_{\text{com}}(t) L_{B/E}^{\top} \boldsymbol{T}_{IBc} \tag{12}$$

where the vector $\boldsymbol{T}_{IBc}$ is defined according to Eq. (8) with $\lambda$ and $\vartheta$ replaced by $\lambda_{\text{com}}(t)$ and $\vartheta_{\text{com}}(t)$, respectively. In general, the reference commands are functions of time that are assumed to be bounded and smooth. In particular, for the formation flight $\boldsymbol{R}_{\text{com}} =$ constant and for the target interception problem $\boldsymbol{R}_{\text{com}} = 0$. In any case these commands must be scaled by the unknown parameter $b_T$ to match the scaled relative dynamics in system (10).

The follower's objective is split into two steps: first, to design a guidance law in the form of the inertial velocity command and second, to design the actual control surface deflections $\boldsymbol{u} = \begin{bmatrix} \delta_T & \delta_e & \delta_a & \delta_r \end{bmatrix}^{\top}$ for the follower to implement the guidance law from the first step. Here, as usual, $\delta_T$, $\delta_e$, $\delta_a$, and $\delta_r$ are, respectively, the follower's throttle, elevator, aileron, and rudder deflections. To this end, we formulate the guidance problem viewing the follower's velocity $\boldsymbol{V}_F(t)$ as the control input and the target's velocity $\boldsymbol{V}_T(t)$ as an unknown time-varying disturbance.

*Problem 1*. Design a guidance law $\boldsymbol{V}_F(t)$ such that the scaled relative position vector $\boldsymbol{r}(t)$ tracks the reference command $\boldsymbol{r}_{\text{com}}(t)$ regardless of the realization of the target's velocity $\boldsymbol{V}_T(t)$, subject to the following assumption.

*Assumption 1*. Assume that the target's inertial velocity $\boldsymbol{V}_T(t)$ is a bounded function of time and has a bounded time derivative, i.e., $\boldsymbol{V}_T(t), \dot{\boldsymbol{V}}_T(t) \in \mathcal{L}_\infty$. Furthermore, assume that any maneuver made by the target is such that the velocity returns to some constant value in finite time or asymptotically in infinite time with a rate sufficient for the integral of the magnitude of velocity change to be finite. □

Because $b_T$ is just a constant, for the convenience in proofs, this assumption is formulated for the function $(1/b_T)\boldsymbol{V}_T(t)$ as follows:

$$\frac{1}{b_T}\boldsymbol{V}_T(t) = \boldsymbol{d} + \boldsymbol{\delta}(t) \tag{13}$$

where $\boldsymbol{d} \in \mathbb{R}^3$ is an unknown but otherwise constant vector and $\boldsymbol{\delta}(t) \in \mathcal{L}_2$ is an unknown time-varying term. For example, any obstacle or collision avoidance can be viewed as such a maneuver, provided that after the maneuver the target velocity returns to a constant in finite time or asymptotically in infinite time subject to $\boldsymbol{\delta}(t) \in \mathcal{L}_2(\mathbb{R}^3)$. Because $\boldsymbol{V}_T(t)$, $\dot{\boldsymbol{V}}_T(t) \in \mathcal{L}_\infty$, it follows that $\boldsymbol{\delta}(t)$, $\dot{\boldsymbol{\delta}}(t) \in \mathcal{L}_\infty$. Therefore, applying the corollary of Barbalat's lemma from [22] (p. 19), we conclude that

$$\boldsymbol{\delta}(t) \to 0, \qquad t \to \infty \tag{14}$$

From the control theoretical point of view, this problem can be considered in the state feedback framework as a simultaneous tracking and disturbance rejection problem for a multi-input multi-output linear system with positive but unknown high-frequency gain in each control channel. In addition, the reference command $\boldsymbol{r}_{\text{com}}(t)$ depends upon the unknown parameter $b_T$. The solution to this problem is the inertial velocity command for the follower that guarantees an asymptotic tracking.

The second problem is formulated as follows.

*Problem 2*. Design a control surface deflection command $\boldsymbol{u} = \begin{bmatrix} \delta_T & \delta_e & \delta_a & \delta_r \end{bmatrix}^{\top}$ such that the follower's inertial velocity tracks the guidance command $\boldsymbol{V}_F(t)$ regardless of the modeling uncertainties and atmospheric turbulence resulting from the target's motion.

The solution to this problem will require translation of the guidance law into a reference command, more convenient for the flight control design.

*Remark 1*. We note that the conventional guidance laws require the measurements of relative range, the line of sight angle rate, the knowledge of time to go, and the target's acceleration bound. These quantities cannot be measured by a single camera, which is assumed to be the only sensor giving information about the target's dynamics.

## III. Guidance Law

### A. Disturbance Rejection Guidance Law for Known Reference Commands

Let $\boldsymbol{r}_{\text{com}}(t)$ be a continuously differentiable bounded known reference signal of interest to track. This corresponds to the case in which the target's size is known. The controller developed in [20] rejects time-varying disturbances $\boldsymbol{\delta}(t) \in \mathcal{L}_2 \bigcap \mathcal{L}_\infty$. Here, using the projection-based classical adaptive laws from [23], we estimate the constant disturbance $\boldsymbol{d}$ and reject $\boldsymbol{\delta}(t)$, simultaneously. The tracking guidance law is defined by

$$\begin{aligned} \boldsymbol{V}_F(t) &= \hat{b}(t)\boldsymbol{g}(t) \\ \boldsymbol{g}(t) &= k\boldsymbol{e}(t) + \hat{\boldsymbol{d}}(t) - \dot{\boldsymbol{r}}_{\text{com}}(t) \end{aligned} \tag{15}$$

where $\boldsymbol{e}(t) = \boldsymbol{r}(t) - \boldsymbol{r}_{\text{com}}(t) \in \mathbb{R}^3$ is the tracking error, $\hat{b}(t) \in \mathbb{R}$ and $\hat{\boldsymbol{d}}(t) \in \mathbb{R}^3$ are the estimates of the unknown parameter $b_T$, and the nominal disturbance $\boldsymbol{d}$, respectively, $k > 0$ is the control gain. Substituting the guidance law from Eq. (15) into relative dynamics in system (10), the error dynamics can be written as

$$\dot{\boldsymbol{e}}(t) = \boldsymbol{d} + \boldsymbol{\delta}(t) - k\boldsymbol{e}(t) - \hat{\boldsymbol{d}}(t) - \frac{\tilde{b}(t)}{b_T}\boldsymbol{g}(t) \tag{16}$$

The adaptive laws for the estimates $\hat{b}(t)$ and $\hat{\boldsymbol{d}}(t)$ are given as follows:

$$\begin{aligned} \dot{\hat{b}}(t) &= \sigma \text{Proj}(\hat{b}(t), \boldsymbol{e}^{\top}(t)\boldsymbol{g}(t)), \qquad \hat{b}(0) = \hat{b}_0 > 0 \\ \dot{\hat{\boldsymbol{d}}}(t) &= G\text{Proj}(\hat{\boldsymbol{d}}(t), \boldsymbol{e}(t)), \qquad \hat{\boldsymbol{d}}(0) = \hat{\boldsymbol{d}}_0 \end{aligned} \tag{17}$$

where $\sigma > 0$ is a constant (adaptation gain), $G$ is a positive definite matrix (adaptation gain), and $\text{Proj}(\cdot,\cdot)$ denotes the projection operator [23] (see Appendix).

Now we are ready to state the main theorem.

*Theorem 1*. The adaptive guidance law given by Eqs. (15) and (17) guarantees global uniform ultimate boundedness of all error signals in the systems (16) and (17) and asymptotic tracking of the reference trajectory $\boldsymbol{r}_{\text{com}}(t)$. □

*Proof*. Letting $\tilde{b}(t) = \hat{b}(t) - b_T$ and $\tilde{\boldsymbol{d}}(t) = \hat{\boldsymbol{d}}(t) - \boldsymbol{d}$, the error dynamics take the form

$$\dot{\boldsymbol{e}}(t) = -k\boldsymbol{e}(t) - \tilde{\boldsymbol{d}}(t) + \boldsymbol{\delta}(t) - \frac{\tilde{b}(t)}{b_T}\boldsymbol{g}(t) \tag{18}$$

Consider the following Lyapunov function candidate:

$$V_1(\boldsymbol{e}, \tilde{b}, \tilde{\boldsymbol{d}}) = \frac{1}{2}\boldsymbol{e}^{\top}(t)\boldsymbol{e}(t) + \frac{1}{2\sigma b_T}\tilde{b}^2(t) + \frac{1}{2}\tilde{\boldsymbol{d}}^{\top}(t)G^{-1}\tilde{\boldsymbol{d}}(t)$$

Its derivative along the trajectories of the systems (15) and (16) has the form

$$\dot{V}_1(t) = -k\boldsymbol{e}^\top(t)\boldsymbol{e}(t) - \boldsymbol{e}^\top(t)\tilde{\boldsymbol{d}}(t) - \frac{\tilde{b}(t)}{b_T}\boldsymbol{e}^\top(t)\boldsymbol{g}(t) + \boldsymbol{e}^\top(t)\boldsymbol{\delta}(t) + \frac{\tilde{b}(t)}{\sigma b_T}\dot{\hat{b}}(t) + \tilde{\boldsymbol{d}}^\top(t)G^{-1}\dot{\hat{\boldsymbol{d}}}(t) = -k\boldsymbol{e}^\top(t)\boldsymbol{e}(t) + \boldsymbol{e}^\top(t)\boldsymbol{\delta}(t) + \frac{\tilde{b}(t)}{b_T}[-\boldsymbol{e}^\top(t)\boldsymbol{g}(t) + \mathrm{Proj}(\hat{b}(t), \boldsymbol{e}^\top(t)\boldsymbol{g}(t))] + \tilde{\boldsymbol{d}}^\top(t)[-\boldsymbol{e}(t) + \mathrm{Proj}(\hat{\boldsymbol{d}}(t), \boldsymbol{e}(t))] \tag{19}$$

Using the properties in Eqs. (A8) and (A10) (see Appendix) and completing the squares in Eq. (19), the following inequality can be written:

$$\dot{V}_1(t) \le -k_1\|\boldsymbol{e}(t)\|^2 + c_1^2\|\boldsymbol{\delta}(t)\|^2 \tag{20}$$

where $c_1$ is a positive constant such that $k_1 = k - 1/(4c_1^2) > 0$. In the preceding derivation, the following inequality has been used:

$$\boldsymbol{e}^\top\boldsymbol{\delta} \le \frac{1}{4c_1^2}\boldsymbol{e}^\top\boldsymbol{e} + c_1^2\boldsymbol{\delta}^\top\boldsymbol{\delta}$$

Because $\boldsymbol{\delta}(t) \in \mathcal{L}_\infty$, there exists some $\rho > 0$ such that $c_1 \| \boldsymbol{\delta}(t) \| \le \rho$. Also, from the inequalities in Eqs. (A8) and (A10), it follows that $\|\tilde{b}(t)\| \le \tilde{b}_*$ and $\|\tilde{\boldsymbol{d}}(t)\| \le \tilde{d}_*$, where $\tilde{b}_*$ and $\tilde{d}_*$ are some positive constants. From the relationship in Eq. (20), it follows that $\dot{V}_1(t) \le 0$ outside the compact set

$$\Omega = \{(\boldsymbol{e}, \tilde{b}, \tilde{\boldsymbol{d}}) \colon \|\boldsymbol{e}\| \le \frac{\rho}{\sqrt{k_1}}, \qquad \|\tilde{b}(t)\| \le \tilde{b}_*, \qquad \|\tilde{\boldsymbol{d}}(t)\| \le \tilde{d}_*\}$$

Hence, all the signals $\boldsymbol{e}(t)$, $\tilde{b}(t)$, $\tilde{\boldsymbol{d}}(t)$, $\boldsymbol{g}(t)$ in the systems (15) and (16) are uniformly ultimately bounded. From Eq. (18), it follows that $\dot{\boldsymbol{e}}(t)$ is bounded. Integrating Eq. (20), we get

$$\int_0^t k_1\|\boldsymbol{e}(\tau)\|^2\,\mathrm{d}\tau \le V_1(0) - V_1(t) + \int_0^t c_1^2\|\boldsymbol{\delta}(\tau)\|^2\,\mathrm{d}\tau \le V_1(0) + \int_0^t c_1^2\|\boldsymbol{\delta}(\tau)\|^2\,\mathrm{d}\tau \tag{21}$$

Because $\boldsymbol{\delta}(t) \in \mathcal{L}_2$, from Eq. (21) we have

$$\lim_{t\to\infty}\int_0^t k_1\|\boldsymbol{e}(\tau)\|^2\,\mathrm{d}\tau < \infty \tag{22}$$

Thus, $\boldsymbol{e}(t) \in \mathcal{L}_2(\mathbb{R}^3) \bigcap \mathcal{L}_\infty(\mathbb{R}^3)$. Also, the error dynamics in Eq. (18) imply that $\dot{\boldsymbol{e}}(t) \in \mathcal{L}_\infty(\mathbb{R}^3)$. Application of Barbalat's lemma [22] ensures that $\boldsymbol{e}(t) \to 0$ as $t \to \infty$, and therefore, $\boldsymbol{r}(t) \to \boldsymbol{r}_{\mathrm{com}}(t)$ as $t \to \infty$. The proof is complete.

### B. Visual Guidance Law

In the case of visual measurement, as discussed in the preceding section, $\boldsymbol{r}_{\mathrm{com}}(t)$ depends upon the unknown geometric size of the target, and therefore is not available for the guidance law in Eq. (15). For the given reference commands $\boldsymbol{R}_{\mathrm{com}}(t)$, one can consider estimated reference commands $\hat{\boldsymbol{r}}_{\mathrm{com}}(t)$ using $\hat{b}(t)$ as follows:

$$\hat{\boldsymbol{r}}_{\mathrm{com}}(t) = \frac{1}{\hat{b}(t)}\boldsymbol{R}_{\mathrm{com}}(t) \tag{23}$$

From the inequality in Eq. (A10) it follows that $\hat{b}(t)$ is bounded away from zero, hence the estimated reference command $\hat{\boldsymbol{r}}_{\mathrm{com}}(t)$ is well defined. Moreover, it is continuously differentiable, with its derivative calculated as follows:

$$\dot{\hat{\boldsymbol{r}}}_{\mathrm{com}}(t) = \frac{1}{\hat{b}(t)}\dot{\boldsymbol{R}}_{\mathrm{com}}(t) - \frac{1}{\hat{b}^2(t)}\dot{\hat{b}}(t)\boldsymbol{R}_{\mathrm{com}}(t) \tag{24}$$

According to Theorem 1, the guidance law in Eq. (15) with $\boldsymbol{r}_{\mathrm{com}}(t)$ replaced by $\hat{\boldsymbol{r}}_{\mathrm{com}}(t)$ and $\dot{\boldsymbol{r}}_{\mathrm{com}}(t)$ replaced by $\dot{\hat{\boldsymbol{r}}}_{\mathrm{com}}(t)$ guarantees the convergence of $\boldsymbol{r}(t)$ to $\hat{\boldsymbol{r}}_{\mathrm{com}}(t)$. However, the convergence of $\boldsymbol{r}(t)$ to $\boldsymbol{r}_{\mathrm{com}}(t)$ is not guaranteed, unless $\hat{\boldsymbol{r}}_{\mathrm{com}}(t)$ converges to $\boldsymbol{r}_{\mathrm{com}}(t)$. The latter can take place in the presence of parameter convergence, i.e., when the parameter estimate $\hat{b}(t)$ converges to the true value $b_T$. Thus, the visual tracking problem can be solved if one ensures that $\hat{b}(t) \to b_T$ as $t \to \infty$. A discussion on this is provided in the next section. First, we need the following auxiliary result. We need to prove that as $t \to \infty$, the Lyapunov function $V_1(t)$ has a finite limit.

*Lemma 1*. There exists a constant $\bar{V}_1 \ge 0$ such that

$$\lim_{t\to\infty} V_1[\boldsymbol{e}(t), \tilde{b}(t), \tilde{\boldsymbol{d}}(t)] = \bar{V}_1$$

□

*Proof*. Introduce a function $s(t)$ as follows:

$$s(t) = -\dot{V}_1(t) - k_1\|\boldsymbol{e}(t)\|^2 + c_1^2\|\boldsymbol{\delta}(t)\|^2 \tag{25}$$

From the upper bound in Eq. (20), it follows that $s(t) \ge 0$. This implies that

$$\int_0^t s(\tau)\,\mathrm{d}\tau$$

is a monotonous (nondecreasing) function of $t$. Integration of the equation in Eq. (25) results in

$$\int_0^t s(\tau)\,\mathrm{d}\tau = -V_1(t) + V_1(0) + \int_0^t\left[-k_1\|\boldsymbol{e}(\tau)\|^2 + c_1^2\|\boldsymbol{\delta}(\tau)\|^2\right]\mathrm{d}\tau \tag{26}$$

It follows from Theorem 1 that $V_1(t)$ is bounded, whereas $\boldsymbol{e}(t)$, $\boldsymbol{\delta}(t) \in \mathcal{L}_2$. Therefore,

$$\int_0^t s(\tau)\,\mathrm{d}\tau$$

is bounded. Hence,

$$\lim_{t\to\infty}\int_0^t s(\tau)\,\mathrm{d}\tau$$

exists. Therefore,

$$\bar{V}_1 = \lim_{t\to\infty} V_1(t) = V_1(0) - \lim_{t\to\infty}\int_0^t s(\tau)\,\mathrm{d}\tau + \lim_{t\to\infty}\int_0^t\left[-k_1\|\boldsymbol{e}(\tau)\|^2 + c_1^2\|\boldsymbol{\delta}(\tau)\|^2\right]\mathrm{d}\tau \tag{27}$$

also exists. The proof is complete.

## IV. Parameter Convergence

Theorem 1 guarantees convergence of the tracking error $\boldsymbol{e}(t)$ to zero but not of the estimation errors $\tilde{b}(t)$ or $\tilde{\boldsymbol{d}}(t)$. Instead, it guarantees convergence of $\dot{\tilde{b}}(t)$ and $\dot{\tilde{\boldsymbol{d}}}(t)$ to zero. In this section, we prove that if $\dot{\hat{\boldsymbol{r}}}_{\mathrm{com}}(t) \to 0$ as $t \to \infty$, then the parameter estimates $\hat{b}(t)$ and $\hat{\boldsymbol{d}}(t)$ in the systems (15) and (16) converge to some constant values $\bar{b}$ and $\bar{\boldsymbol{d}} = \begin{bmatrix}\bar{d}_x & \bar{d}_y & \bar{d}_z\end{bmatrix}^\top$, respectively, but not necessarily to the true values $b_T$ and $\boldsymbol{d}$. To prove this result, we need the following Extended Barbalat's lemma from [24]:

*Lemma 2 (Extended Barbalat's lemma)*. Let $\varphi(t)$ be a real piecewise continuous function of real variable $t$ and defined for $t \ge t_0$, $t_0 \in \mathbb{R}$. Assume that $\varphi(t)$ can be decomposed as $\varphi(t) = \varphi_1(t) + \varphi_2(t)$, where $\varphi_1(t)$ is uniformly continuous for $t \ge t_0$ and $\varphi_2(t)$ satisfies

$$\lim_{t\to\infty}\varphi_2(t) = 0$$

If

$$\lim_{t\to\infty}\int_{t_0}^{t}\varphi(\tau)\,\mathrm{d}\tau$$

exists and is finite, then

$$\lim_{t\to\infty}\varphi(t)=0$$

□

A proof of this lemma is given in [24].

*Lemma 3*. The adaptive controller in Eqs. (15) and (17) guarantees convergence of parameter estimates $\hat{b}(t)$ and $\hat{\boldsymbol{d}}(t)$ to constant values, provided that $\dot{\hat{\boldsymbol{r}}}_{\mathrm{com}}(t)\to 0$ as $t\to\infty$. □

*Proof*. From Theorem 1 it follows that all the signals in the system are bounded; therefore, $\dot{\hat{b}}(t)$ and $\dot{\hat{\boldsymbol{d}}}(t)$ are bounded, implying uniform continuity of the signals $\hat{b}(t)$, $\tilde{b}(t)$, $\hat{\boldsymbol{d}}(t)$, and $\tilde{\boldsymbol{d}}(t)$. The error dynamics in Eq. (16) can be written in the form

$$\dot{\boldsymbol{e}}(t)=\boldsymbol{\varphi}_1(t)+\boldsymbol{\varphi}_2(t) \tag{28}$$

where

$$\boldsymbol{\varphi}_1(t)=-\tilde{\boldsymbol{d}}(t)-\frac{\tilde{b}(t)}{b_T}\hat{\boldsymbol{d}}(t)$$

$$\boldsymbol{\varphi}_2(t)=\left(-1-\frac{\tilde{b}(t)}{b_T}\right)k\boldsymbol{e}(t)+\boldsymbol{\delta}(t)+\frac{\tilde{b}(t)}{b_T}\dot{\hat{\boldsymbol{r}}}_{\mathrm{com}}(t)$$

The function $\boldsymbol{\varphi}_1(t)$ is uniformly continuous because it is a sum of uniformly continuous functions. Also, because $\boldsymbol{e}(t)\to 0$, $\boldsymbol{\delta}(t)\to 0$, and $\dot{\hat{\boldsymbol{r}}}_{\mathrm{com}}(t)\to 0$, then $\boldsymbol{\varphi}_2(t)\to\boldsymbol{0}$ as $t\to\infty$. Thus, the error $\boldsymbol{e}(t)$ has a finite limit as $t\to\infty$, and application of Lemma 2 implies that $\dot{\boldsymbol{e}}(t)\to 0$ as $t\to\infty$. Hence, as $t\to\infty$, the error dynamics in Eq. (28) reduce to

$$\tilde{\boldsymbol{d}}(t)+\frac{\tilde{b}(t)}{b_T}\hat{\boldsymbol{d}}(t)\to\boldsymbol{0} \tag{29}$$

With $\hat{\boldsymbol{d}}(t)=\boldsymbol{d}+\tilde{\boldsymbol{d}}(t)$, the relationship in Eq. (29) can be transformed into

$$\hat{b}(t)\tilde{\boldsymbol{d}}(t)+\tilde{b}(t)\boldsymbol{d}\to\boldsymbol{0},\qquad t\to\infty \tag{30}$$

Fix arbitrary $\varepsilon>0$. The limit in Eq. (30) implies that there exists a time instance $T_1(\varepsilon)$ such that for all $t>T_1(\varepsilon)$

$$\|\hat{b}(t)\tilde{\boldsymbol{d}}(t)+\tilde{b}(t)\boldsymbol{d}\|<\varepsilon \tag{31}$$

We recall that according to the inequality in Eq. (A10), $\hat{b}(t)\geq b_{\min}>0$ for every $t>0$. Let $t>T_1(\varepsilon)$. The relationship in Eq. (31) can be written componentwise, e.g., for $x$, as follows:

$$|\hat{b}(t)\tilde{d}_x(t)+\tilde{b}(t)d_x|<\varepsilon \tag{32}$$

Upon some algebra in Eq. (32), the following inequality can be derived:

$$\frac{\tilde{b}^2(t)}{\hat{b}^2(t)}d_x^2-\zeta_x(\varepsilon)<\tilde{d}_x^2(t)<\frac{\tilde{b}^2(t)}{\hat{b}^2(t)}d_x^2+\zeta_x(\varepsilon) \tag{33}$$

where

$$\zeta_x(\varepsilon)=\frac{|\varepsilon^2+2\varepsilon d_x|}{b_{\min}^2}$$

and obviously $\zeta_x(\varepsilon)\to 0$ as $\varepsilon\to 0$. The same type of inequalities can be written for the other two components of $\tilde{\boldsymbol{d}}(t)$. From Lemma 1, it follows that for the same $\varepsilon$ chosen in the preceding equations, there exists a time instance $T_2(\varepsilon)$ such that for $t>T_2(\varepsilon)$

$$\left|\frac{1}{2\sigma b_T}\tilde{b}^2(t)+\frac{1}{2}\tilde{\boldsymbol{d}}^{\top}(t)G^{-1}\tilde{\boldsymbol{d}}(t)-\bar{V}_1\right|<\varepsilon \tag{34}$$

For the given $\varepsilon$, the time instances $T_1(\varepsilon)$ and $T_2(\varepsilon)$ may be different. Choosing the largest one and denoting $T_3(\varepsilon)=\max[T_1(\varepsilon),T_2(\varepsilon)]$, all of the preceding and the following conclusions remain valid for all $t>T_3(\varepsilon)$.

Let $G$ be a diagonal matrix with positive elements $g_{11}, g_{22}, g_{33}$ on the main diagonal. This is usually the case for the adaptive gains in the update laws. Then, taking into account the inequality in Eq. (33), it follows from the inequality in Eq. (34) that for all $t>T_3(\varepsilon)$

$$\left|\frac{1}{2\sigma b_T}\tilde{b}^2(t)+\frac{1}{2}\boldsymbol{d}^{\top}G^{-1}\boldsymbol{d}\frac{\tilde{b}^2(t)}{\hat{b}^2(t)}-\bar{V}_1\right|<\varepsilon+\zeta(\varepsilon) \tag{35}$$

where

$$\zeta(\varepsilon)=\frac{1}{2}[g_{11}\zeta_x(\varepsilon)+g_{22}\zeta_y(\varepsilon)+g_{33}\zeta_z(\varepsilon)]$$

which implies that

$$[b_T+\tilde{b}(t)]^2\tilde{b}^2(t)+c_2\tilde{b}^2(t)-c_3[b_T+\tilde{b}(t)]^2\to 0 \tag{36}$$

where $c_2=b_T\sigma\boldsymbol{d}^{\top}G^{-1}\boldsymbol{d}>0$, $c_3=2\sigma b_T\bar{V}_1>0$. Consider the function $p(\xi)=(b_T+\xi)^2\xi^2+c_2\xi^2-c_3(b_T+\xi)^2$. It is a monic polynomial of fourth order in $\xi$, and takes a negative value at $\xi=0$. Therefore, it has at least two real roots. In general, it can be represented in the case of four real roots as $p(\xi)=(\xi-b_1)(\xi-b_2)(\xi-b_3)(\xi-b_4)$ or in the case of two real roots as $p(\xi)=(\xi-b_1)(\xi-b_2)q(\xi)$, where $q(\xi)$ is a monic quadratic polynomial with no real roots. Thus, there exists some positive constant $\nu$, such that $q(\xi)\geq\nu$ for all values of $\xi$. First, consider the case of four real roots. The relationship in Eq. (36) implies that for an arbitrary positive number $\varepsilon$, there exists a time instance $T_3(\varepsilon)$, such that for all $t>T_3(\varepsilon)$

$$|[\tilde{b}(t)-b_1][\tilde{b}(t)-b_2][\tilde{b}(t)-b_3][\tilde{b}(t)-b_4]|<\varepsilon \tag{37}$$

or, equivalently,

$$|\tilde{b}(t)-b_1||\tilde{b}(t)-b_2||\tilde{b}(t)-b_3||\tilde{b}(t)-b_4|<\varepsilon \tag{38}$$

This implies that

$$|\tilde{b}(t)-b_k|=\min_i[|\tilde{b}(t)-b_i|,\quad i=1,\ldots,4]<\varepsilon^{1/4} \tag{39}$$

Because $\varepsilon$ is an arbitrarily small number, the inequality in Eq. (39) implies that $\tilde{b}(t)\to b_k$ as $t\to\infty$. Notice, that because $\tilde{b}(t)$ is a continuous function, it cannot simultaneously converge to two distinct constants. That is, only one of the factors in Eq. (38) can be arbitrarily small. The case of two real roots can be handled similarly. This implies that the parameter error $\tilde{b}(t)$ converges to some constant value, and so does the parameter estimate $\hat{b}(t)$, that is, $\hat{b}(t)\to\bar{b}$ as $t\to\infty$, where $\bar{b}$ is some constant. From Eq. (30) it follows that $\hat{\boldsymbol{d}}(t)$ converges to some constant vector $\bar{\boldsymbol{d}}$ as well.

*Remark 2*. In the special case of formation flight, the reference command $\boldsymbol{R}_{\mathrm{com}}$ is constant. From Theorem 1 it follows that $\dot{\tilde{b}}(t)\to 0$ as $t\to\infty$, implying that $\dot{\hat{b}}(t)\to 0$. Then, the relationships in Eq. (24) imply that $\dot{\hat{\boldsymbol{r}}}_{\mathrm{com}}(t)\to 0$ as $t\to\infty$. □

Lemma 3 states that the parameter estimates converge to a point within the set described by the equation $\bar{b}\,\bar{\boldsymbol{d}}=b_T\boldsymbol{d}$, if $\dot{\hat{\boldsymbol{r}}}_{\mathrm{com}}(t)\to 0$ as $t\to\infty$. However, $\bar{b}=b_T$ and $\bar{\boldsymbol{d}}=\boldsymbol{d}$ are not guaranteed. Thus, for the convergence of parameter estimates to true values, we need to provide some excitation in the form of sinusoidal components in the reference signal to prevent $\dot{\hat{\boldsymbol{r}}}_{\mathrm{com}}(t)\to 0$ [25]. The next lemma shows that in the special case of formation flight, exciting the reference command $\boldsymbol{R}_{\mathrm{com}}$ only in one direction is sufficient for the convergence of all the parameters to their respective true values. Thus, for the given constant reference command $\boldsymbol{R}_{\mathrm{com}}$ the "excited" reference command is defined as follows:

$$\boldsymbol{R}^{*}_{\mathrm{com}}(t)=\boldsymbol{R}_{\mathrm{com}}+a\sin(\omega t)\boldsymbol{E} \tag{40}$$

where $a$ is the excitation amplitude, $\omega$ is the excitation frequency, and the vector $\boldsymbol{E}$ specifies the direction of the excitation. For instance, we can excite only the reference command in the $x$ direction by setting $\boldsymbol{E} = [1 \quad 0 \quad 0]^\top$.

*Lemma 4*. If $\boldsymbol{R}_{\text{com}}$ is constant, then for the reference command $\boldsymbol{R}^*_{\text{com}}(t)$, the adaptive controller in Eq. (15) guarantees the convergence of parameter errors to zero. □

*Proof*. The adaptive controller in Eq. (15) guarantees the convergence of the tracking error to zero as $t \to \infty$ (Theorem 1), which consequently implies that $\dot{\hat{b}}(t) \to 0$. According to the equations in Eq. (24), the derivative of the estimated reference command $\dot{\hat{\boldsymbol{r}}}_{\text{com}}(t)$ is represented as a sum of two terms: $\dot{\hat{\boldsymbol{r}}}_{\text{com}}(t) = \dot{\hat{\boldsymbol{r}}}_{\text{com1}}(t) + \dot{\hat{\boldsymbol{r}}}_{\text{com2}}(t)$, where

$$\dot{\hat{\boldsymbol{r}}}_{\text{com1}}(t) = \frac{1}{\hat{b}(t)} a\omega \cos(\omega t)\boldsymbol{E}, \qquad \dot{\hat{\boldsymbol{r}}}_{\text{com2}}(t) = -\frac{\dot{\hat{b}}(t)}{\hat{b}^2(t)} \boldsymbol{R}^*_{\text{com}}(t)$$

It is easy to see that $\dot{\hat{\boldsymbol{r}}}_{\text{com1}}(t)$ is uniformly continuous, because $1/\hat{b}(t)$ and $\cos(\omega t)$ are uniformly continuous, and $\dot{\hat{\boldsymbol{r}}}_{\text{com2}}(t) \to 0$ as $t \to \infty$, because $\hat{b}(t)$ is bounded away from zero and $\dot{\hat{b}}(t) \to 0$. Thus, the error dynamics in Eq. (16) can be represented as

$$\dot{\boldsymbol{e}}(t) = \boldsymbol{\varphi}_1(t) + \boldsymbol{\varphi}_2(t) \tag{41}$$

where

$$\boldsymbol{\varphi}_1(t) = -\tilde{\boldsymbol{d}}(t) - \frac{\tilde{b}(t)}{b_T}[\hat{\boldsymbol{d}}(t) - \dot{\hat{\boldsymbol{r}}}_{\text{com1}}(t)]$$

is uniformly continuous, whereas

$$\boldsymbol{\varphi}_2(t) = \left(-1 - \frac{\tilde{b}(t)}{b_T}\right) k\boldsymbol{e}(t) + \boldsymbol{\delta}(t) + \frac{\tilde{b}(t)}{b_T} \dot{\hat{\boldsymbol{r}}}_{\text{com2}}(t) \to \boldsymbol{0}$$

as $t \to \infty$. Application of Extended Barbalat's lemma implies that $\dot{\boldsymbol{e}}(t) \to \boldsymbol{0}$ as $t \to \infty$. Therefore, the error dynamics reduce to

$$-\tilde{\boldsymbol{d}}(t) - \frac{\tilde{b}(t)}{b_T}[\hat{\boldsymbol{d}}(t) - \dot{\hat{\boldsymbol{r}}}_{\text{com1}}(t)] \to \boldsymbol{0}, \qquad t \to \infty \tag{42}$$

Without loss of generality, we let $\boldsymbol{E} = \begin{bmatrix} 1 & 0 & 0 \end{bmatrix}^\top$. Consider the $x$ component of the vector relationship in Eq. (42):

$$\tilde{d}_x(t) + \frac{\tilde{b}(t)}{b_T}\left[\hat{d}_x(t) - \frac{a\omega}{\hat{b}(t)}\cos(\omega t)\right] \to 0 \tag{43}$$

With the help of $\hat{\boldsymbol{d}}(t) = \boldsymbol{d} + \tilde{\boldsymbol{d}}(t)$ and $\hat{b}(t) = b_T + \tilde{b}(t)$, it can be transformed into the form

$$\hat{b}(t)\tilde{d}_x(t) + \tilde{b}(t)\left[d_x - \frac{a\omega}{\hat{b}(t)}\cos(\omega t)\right] \to 0 \tag{44}$$

which can be equivalently written in inner product form as follows:

$$\begin{bmatrix} \hat{b}(t) \\ d_x - \frac{a\omega}{\hat{b}(t)}\cos(\omega t) \end{bmatrix}^\top \begin{bmatrix} \tilde{d}_x(t) \\ \tilde{b}(t) \end{bmatrix} \to 0 \tag{45}$$

We note that the vector

$$\boldsymbol{h}(t) = \begin{bmatrix} \hat{b}(t) & d_x - \frac{a\omega}{\hat{b}(t)}\cos(\omega t) \end{bmatrix}^\top$$

is persistently exciting, i.e., there exists positive constants $c_4$, $c_5$, $T$ such that the inequalities

$$c_4 \geq \int_t^{t+T} [\boldsymbol{h}^\top(\tau)\boldsymbol{\xi}^e]^2 \, \mathrm{d}\tau \geq c_5 \tag{46}$$

hold for all $\boldsymbol{\xi}^e = \begin{bmatrix} \xi^e_1 & \xi^e_2 \end{bmatrix}^\top$ with $\|\boldsymbol{\xi}^e\| = 1$ and $t \geq 0$. Indeed, the left side of the inequality in Eq. (46) follows from the fact that all the signals in the system are bounded; hence, there exists a positive constant $c_6$ such that $\|\boldsymbol{h}(t)\| \leq c_6$. Therefore,

$$\int_t^{t+T} [\boldsymbol{h}^\top(\tau)\boldsymbol{\xi}^e]^2 \, \mathrm{d}\tau \leq \int_t^{t+T} \|\boldsymbol{h}^\top(\tau)\|^2 \|\boldsymbol{\xi}^e\|^2 \, \mathrm{d}\tau \leq c_6^2 T$$

And so, $c_4$ can be chosen equal to $c_6^2 T$. To prove the right-hand side of the inequality in Eq. (46), we write

$$\begin{aligned} I(t,T) = \int_t^{t+T} [\boldsymbol{h}^\top(\tau)\boldsymbol{\xi}^e]^2 \, \mathrm{d}\tau &= \int_t^{t+T} \left[\xi^e_1 \hat{b}(\tau) + \xi^e_2 \, \mathrm{d}_x\right]^2 \mathrm{d}\tau \\ &+ a^2\omega^2 \left(\xi^e_2\right)^2 \int_t^{t+T} \frac{1}{\hat{b}^2(\tau)} \cos^2(\omega\tau) \, \mathrm{d}\tau \\ &- 2a\omega\xi^e_1\xi^e_2 \int_t^{t+T} \cos(\omega\tau) \, \mathrm{d}\tau \\ &- 2a\omega\left(\xi^e_2\right)^2 \mathrm{d}_x \int_t^{t+T} \frac{1}{\hat{b}(\tau)} \cos(\omega\tau) \, \mathrm{d}\tau \end{aligned} \tag{47}$$

From the inequality in Eq. (A10), we deduce the following lower bound for the integral $I(t,T)$:

$$\begin{aligned} I(t,T) \geq \int_t^{t+T} \left[\xi^e_1 \hat{b}(\tau) + \xi^e_2 \, \mathrm{d}_{0x}\right]^2 \mathrm{d}\tau &\\ + a^2\omega^2 \left(\xi^e_2\right)^2 \frac{1}{b^2_{\max}} \int_t^{t+T} \cos^2(\omega\tau) \, \mathrm{d}\tau &\\ - 2a\omega\xi^e_1\xi^e_2 \int_t^{t+T} \cos(\omega\tau) \, \mathrm{d}\tau &\\ - 2a\omega\left(\xi^e_2\right)^2 \mathrm{d}_x \frac{1}{b_{\min}} \int_t^{t+T} \cos(\omega\tau) \, \mathrm{d}\tau & \end{aligned} \tag{48}$$

Choosing $T = (2\pi/\omega)m$, where $m$ is any positive integer, renders

$$\int_t^{t+T} \cos(\omega\tau) \, \mathrm{d}\tau = 0, \qquad \int_t^{t+T} \cos^2(\omega\tau) \, \mathrm{d}\tau = \frac{T}{2}$$

Therefore,

$$I(t,T) \geq \int_t^{t+T} [\xi^e_b \hat{b}(\tau) + \xi^e_2 \, \mathrm{d}_{0x}]^2 \, \mathrm{d}\tau + \frac{a^2\omega^2\left(\xi^e_2\right)^2}{2b^2_{\max}} T$$

It is easy to see that if $\xi^e_2 = 0$, then $\xi^e_1 = 1$

$$I(t,T) \geq \int_t^{t+T} \hat{b}^2(\tau) \, \mathrm{d}\tau \geq T b^2_{\min}$$

otherwise

$$I(t,T) \geq \frac{a^2\omega^2\left(\xi^e_2\right)^2}{2b^2_{\max}} T$$

Hence, for every $\boldsymbol{\xi}^e$ there exists a positive constant $c_5 > 0$ such that $I(t,T) \geq c_5$. Thus, Eq. (46) holds, and therefore, it follows from Eq. (45) that $\tilde{d}_x(t) \to 0$, $\tilde{b}(t) \to 0$ as $t \to \infty$. Then, from the remaining two components of the vector relationship in Eq. (29), it follows that $\tilde{d}_y(t) \to 0$, $\tilde{d}_z(t) \to 0$. Hence, $\hat{b}(t) \to b_T$ and $\hat{\boldsymbol{r}}_{\text{com}}(t) \to (1/b_T)\boldsymbol{R}^*_{\text{com}}(t)$. The proof is complete.

*Remark 3*. In applications, a persistently exciting signal is usually undesirable because it deteriorates the tracking of the constant reference command. Moreover, in visual control, it can easily lose the moving target from the field of view. A recently developed technique of intelligent excitation allows for controlling of the amplitude of the excitation signal, dependent upon the convergence of the output tracking error and parameter errors [12]. It also ensures simultaneous convergence of the parameter and output tracking error to zero. Next, in simulations, we incorporate this technique to ensure parameter convergence. □

*Remark 4*. For the target interception problem, the reference command for the relative range is zero. Therefore $\boldsymbol{r}_{\text{com}} = 0$ and, hence $\dot{\boldsymbol{r}}_{\text{com}} = 0$. Then, the guidance law

$$\begin{aligned} \bar{\boldsymbol{V}}_F^B(t) &= \hat{b}(t)\boldsymbol{g}(t) \\ \boldsymbol{g}(t) &= k\boldsymbol{r}(t) + \hat{\boldsymbol{d}}(t) \\ \dot{\hat{b}}(t) &= \sigma\text{Proj}(\hat{b}(t), \boldsymbol{r}^\top(t)\boldsymbol{g}(t)) \\ \dot{\hat{\boldsymbol{d}}}(t) &= G\text{Proj}(\hat{\boldsymbol{d}}(t), \boldsymbol{r}(t)) \end{aligned} \tag{49}$$

guarantees boundedness of all the signals and convergence of the relative states to zero: $\boldsymbol{r}(t) \to 0$ as $t \to \infty$. There is no need to require parameter convergence, and hence, the need for introducing an excitation signal disappears. □

*Remark 5*. We notice that with two cameras the target's relative position vector $\boldsymbol{R}^B$ can be calculated from both camera measurements, thus removing the unknown parametrization and reducing the problem to simple disturbance rejection for a known system. In this case, the relative range is proportional to the separation of two cameras, whereas in the case of one camera it is proportional to the target's maximum size, as it can be seen from the relationship in Eq. (6). Thus, if the follower has two cameras, the relative range can be estimated with sufficient accuracy if the follower has relatively large wing span; whereas in the case of a MAV or a missile, the second camera may not add any useful information, hence the tracking problem can be solved using the proposed algorithm in this paper.

## V. Measurement Noise

The guidance law derived in the preceding sections assumes availability of perfect measurements from the visual sensor. However, in realistic applications these measurements are corrupted with noise. Therefore, instead of ideal measurements $y_I(t)$, $z_I(t)$, $b_I(t)$ one should consider $y_I^*(t) = y_I(t) + n_y(t)$, $z_I^*(t) = z_I(t) + n_z(t)$, $b_I^*(t) = b_I(t) + n_b(t)$, where $\boldsymbol{n}_I(t) \triangleq [n_y(t) \quad n_z(t) \quad n_b(t)]^\top$ represents the vector of the noise components in the corresponding measurements. Thus, the tracking problem should be addressed with realistic measurements $y_I^*(t)$, $z_I^*(t)$, $b_I^*(t)$. Then the expressions in Eqs. (3) and (6) are written as

$$\begin{aligned} \tan\lambda^*(t) &= \frac{y_I(t) + n_y(t)}{l} \\ \tan\vartheta^*(t) &= \frac{z_I(t) + n_z(t)}{\sqrt{l^2 + [y_I(t) + n_y(t)]^2}} \\ a_I^*(t) &= \frac{\sqrt{l^2 + [y_I(t) + n_y(t)]^2 + [z_I(t) + n_z(t)]^2}}{b_I(t) + n_b(t)} \end{aligned} \tag{50}$$

The measurements of the scaled state vector $\boldsymbol{r}(t)$ are expressed in the following form

$$\boldsymbol{r}^*(t) = L_{E/B}a_I^*(t)\boldsymbol{T}_{BI}^*(\lambda^*(t), \vartheta^*(t)) \triangleq L_{E/B}\boldsymbol{f}(y_I^*(t), z_I^*(t), b_I^*(t)) \tag{51}$$

where the vector $\boldsymbol{T}_{BI}^*(\lambda^*(t), \vartheta^*(t))$ is defined similar to $\boldsymbol{T}_{BI}$ in Eq. (8) with $\lambda$, $\vartheta$ replaced by $\lambda^*$, $\vartheta^*$, respectively. When the noise level is small, one can expand the expressions in Eq. (51) into Taylor series around the ideal measurements $y_I(t)$, $z_I(t)$, $b_I(t)$:

$$\boldsymbol{r}^*(t) = \boldsymbol{r}(t) + L_{E/B}\nabla\boldsymbol{f}(y_I(t), z_I(t), b_I(t))\boldsymbol{n}_I(t) \tag{52}$$

For the uncorrelated, zero-mean, Gaussian, white noise $\boldsymbol{n}_I(t)$ with the correlation matrix $E\{\boldsymbol{n}_I(t)\boldsymbol{n}_I^\top(\tau)\} = \text{diag}(\bar{n}_y, \bar{n}_z, \bar{n}_b)\delta(t-\tau)$, where $E\{\cdot\}$ denotes the mathematical expectation, $\bar{n}_y$, $\bar{n}_z$, $\bar{n}_b$ are positive constants, and $\delta(\cdot)$ is the Dirac delta function, the vector $\boldsymbol{n}_r(t) = L_{E/B}\nabla\boldsymbol{f}(y_I(t), z_I(t), b_I(t))\boldsymbol{n}_I(t)$ also represents a zero-mean Gaussian, white noise process with the correlation matrix $E\{\boldsymbol{n}_r(t)\boldsymbol{n}_r^\top(\tau)\} = S_n(t)\text{diag}(\bar{n}_y, \bar{n}_z, \bar{n}_b)S_n^\top(\tau)\delta(t-\tau)$, where $S_n(t) = L_{E/B}(t)\nabla\boldsymbol{f}(y_I(t), z_I(t), b_I(t))$. Therefore, in the sequel, we will assume that the scaled state vector $\boldsymbol{r}(t)$ is available with the additive, zero-mean, Gaussian, white noise:

$$\boldsymbol{r}^*(t) = \boldsymbol{r}(t) + \boldsymbol{n}_r(t) \tag{53}$$

with the correlation matrix $E\{\boldsymbol{n}_r(t)\boldsymbol{n}_r^\top(\tau)\} = K_{\boldsymbol{n}_r}(t,\tau)\delta(t-\tau)$, $K_{\boldsymbol{n}_r}(t,\tau) > 0$ for all $t, \tau > 0$. To modify the guidance law that can accommodate the measurement noise, we introduce a state estimator for the scaled state vector $\boldsymbol{r}(t)$ as follows:

$$\dot{\hat{\boldsymbol{r}}}(t) = \hat{\boldsymbol{d}}(t) - \boldsymbol{g}(t) + L_f[\boldsymbol{r}^*(t) - \hat{\boldsymbol{r}}(t)] \tag{54}$$

where the function $\boldsymbol{g}(t)$ and hence the guidance law are modified to be

$$\begin{aligned} \boldsymbol{V}_F(t) &= \hat{b}(t)\boldsymbol{g}(t) \\ \boldsymbol{g}(t) &= k[\hat{\boldsymbol{r}}(t) - \boldsymbol{r}_{\text{com}}(t)] + \hat{\boldsymbol{d}}(t) - \dot{\hat{\boldsymbol{r}}}_{\text{com}}(t) \end{aligned} \tag{55}$$

and the gain matrix $L_f$ is chosen to minimize the mean square estimation error

$$J_n = E\{\tilde{\boldsymbol{r}}^\top(t)\tilde{\boldsymbol{r}}(t)\} \tag{56}$$

where $\tilde{\boldsymbol{r}}(t) = \boldsymbol{r}(t) - \hat{\boldsymbol{r}}(t)$ is the estimation error. The estimation error dynamics can be written as follows

$$\dot{\tilde{\boldsymbol{r}}}(t) = -L_f\tilde{\boldsymbol{r}}(t) - \tilde{\boldsymbol{d}}(t) - \frac{\tilde{b}(t)}{b_T}\boldsymbol{g}(t) + \boldsymbol{\delta}(t) - L_f\boldsymbol{n}_r(t) \tag{57}$$

With the modification in guidance law presented in Eq. (55), the tracking error dynamics in Eq. (18) are modified as follows:

$$\dot{\boldsymbol{e}}(t) = -k\boldsymbol{e}(t) + k\tilde{\boldsymbol{r}}(t) - \tilde{\boldsymbol{d}}(t) + \boldsymbol{\delta}(t) - \frac{\tilde{b}(t)}{b_T}\boldsymbol{g}(t) \tag{58}$$

We combine both error dynamics into one equation

$$\dot{\boldsymbol{\xi}}_a(t) = A_a\boldsymbol{\xi}_a(t) + B_a\left[\boldsymbol{\delta}(t) - \tilde{\boldsymbol{d}}(t) - \frac{\tilde{b}(t)}{b_T}\boldsymbol{g}(t)\right] + B_n\boldsymbol{n}_r(t) \tag{59}$$

where

$$\boldsymbol{\xi}_a = \begin{bmatrix} \boldsymbol{e} \\ \tilde{\boldsymbol{r}} \end{bmatrix}, \qquad A_a = \begin{bmatrix} -kI_{3\times3} & kI_{3\times3} \\ 0_{3\times3} & -L_f \end{bmatrix}$$
$$B_a = \begin{bmatrix} I_{3\times3} \\ I_{3\times3} \end{bmatrix}, \qquad B_n = \begin{bmatrix} 0_{3\times3} \\ -L_f \end{bmatrix}$$

The adaptive laws are modified as follows:

$$\begin{aligned} \dot{\hat{b}}(t) &= \sigma\text{Proj}(\hat{b}(t), \boldsymbol{g}(t)^\top B_a^\top P_a\boldsymbol{\xi}_a^*(t)) \\ \dot{\hat{\boldsymbol{d}}}(t) &= G\text{Proj}(\hat{\boldsymbol{d}}(t), B_a^\top P_a\boldsymbol{\xi}_a^*(t)) \end{aligned} \tag{60}$$

where

$$\boldsymbol{\xi}_a^* = \begin{bmatrix} \boldsymbol{r}^* - \boldsymbol{r}_{\text{com}} \\ \boldsymbol{r}^* - \hat{\boldsymbol{r}} \end{bmatrix} = \begin{bmatrix} \boldsymbol{e} + \boldsymbol{n}_r \\ \tilde{\boldsymbol{r}} + \boldsymbol{n}_r \end{bmatrix} = \boldsymbol{\xi}_a + B_a\boldsymbol{n}_r$$

and $P_a$ is a symmetric positive definite matrix that solves the Lyapunov equation

$$A_a^\top P_a + P_aA_a = -Q_a \tag{61}$$

for the Hurwitz matrix $A_a$ and any symmetric positive definite matrix $Q_a$. Next, we prove that for any bounded $\boldsymbol{n}_r(t)$, all the signals in Eqs. (59) and (60) are uniformly ultimately bounded.

*Theorem 2*. If $\boldsymbol{n}_r(t)$ is bounded, the systems (59) and (60) are uniformly ultimately bounded. Moreover, if $\boldsymbol{n}_r(t) = 0$, the combined error $\boldsymbol{\xi}_a(t)$ asymptotically converges to zero. In addition, if the

estimated reference command $\hat{\boldsymbol{r}}_{\text{com}}(t)$ is intelligently exciting, then the parameter errors $\tilde{b}(t)$ and $\tilde{\boldsymbol{d}}(t)$ converge to zero as well.

*Proof.* Consider the following Lyapunov function candidate

$$V_2(\boldsymbol{\xi}_a, \tilde{b}, \tilde{\boldsymbol{d}}) = \boldsymbol{\xi}_a^\top(t) P_a \boldsymbol{\xi}_a(t) + \frac{1}{b_T \sigma} \tilde{b}^2(t) + \tilde{\boldsymbol{d}}^\top(t) G^{-1} \tilde{\boldsymbol{d}}(t)$$

Its derivative along the trajectories of the systems (58–60) has the form

$$\begin{aligned}\dot{V}_2(t) &= \boldsymbol{\xi}_a^\top(t)\left(A_a^\top P_a + P_a A_a\right)\boldsymbol{\xi}_a(t) + 2\boldsymbol{\xi}_a^\top(t) P_a B_a \left[\boldsymbol{\delta}(t) - \tilde{\boldsymbol{d}}(t) \right.\\ &\left. - \frac{\tilde{b}(t)}{b_T}\boldsymbol{g}(t)\right] + 2\boldsymbol{\xi}_a^\top(t) P_a B_n \boldsymbol{n}_r(t) + \frac{2}{\sigma b_T}\tilde{b}(t)\dot{\tilde{b}}(t)\\ &+ 2\tilde{\boldsymbol{d}}^\top(t) G^{-1}\dot{\tilde{\boldsymbol{d}}}(t) = -\boldsymbol{\xi}_a^\top(t) Q_a \boldsymbol{\xi}_a(t) + 2\boldsymbol{\xi}_a^\top(t) P_a B_a \boldsymbol{\delta}(t)\\ &+ 2\boldsymbol{\xi}_a^\top(t) P_a B_n \boldsymbol{n}_r(t) + 2\frac{\tilde{b}(t)}{b_T}\left[-\boldsymbol{g}^\top(t) B_a^\top P_a \boldsymbol{\xi}_a(t) + \frac{1}{\sigma}\dot{\hat{b}}(t)\right]\\ &+ \tilde{\boldsymbol{d}}^\top(t)\left[-B_a^\top P_a \boldsymbol{\xi}_a(t) + G^{-1}\dot{\hat{\boldsymbol{d}}}(t)\right] \end{aligned} \tag{62}$$

Substituting the adaptive laws from Eq. (60), taking into account the definition of $\boldsymbol{\xi}_a^*$ and using the properties of the projection operator in Eqs. (A5) and (A6), the following upper bound can be derived:

$$\begin{aligned}\dot{V}_2(t) &\le -\boldsymbol{\xi}_a^\top(t) Q_a \boldsymbol{\xi}_a(t) + 2\boldsymbol{\xi}_a^\top(t) P_a B_a \boldsymbol{\delta}(t)\\ &+ 2\left(\frac{\tilde{b}(t)}{b_T}\boldsymbol{g} + \boldsymbol{d}(t)\right)^\top B_a^\top P_a B_a \boldsymbol{n}_r(t) + 2\boldsymbol{\xi}_a^\top(t) P_a B_n \boldsymbol{n}_r(t)\end{aligned} \tag{63}$$

From the properties of the projection operator, it follows that $\|\tilde{b}(t)\| \le \tilde{b}_a^*$ and $\|\tilde{\boldsymbol{d}}(t)\| \le \tilde{d}_a^*$, where $\tilde{b}_a^*$ and $\tilde{d}_a^*$ are some positive constants. Therefore, the derivative of $V_2$ can be further upper bounded as follows:

$$\begin{aligned}\dot{V}_2(t) &\le -\lambda_{\min}(Q_a)\|\boldsymbol{\xi}_a(t)\|^2\\ &+ 2\left(\frac{\tilde{b}_a^*}{b_T}\|\boldsymbol{g}\| + \tilde{d}_a^*\right)\|B_a^\top P_a B_a\|\|\boldsymbol{n}_r(t)\|\\ &+ 2\|\boldsymbol{\xi}_a(t)\|\left(\|P_a B_n\|\|\boldsymbol{n}_r(t)\| + \|P_a B_a\|\|\boldsymbol{\delta}(t)\|\right)\end{aligned}$$

where $\lambda_{\min}(Q_a)$ denotes the minimum eigenvalue of the matrix $Q_a$. Because $\dot{\boldsymbol{R}}_{\text{com}}(t)$ is assumed to be bounded, and the projection operator in the adaptive law in Eq. (60) guarantees boundedness of $\hat{b}(t)$ $\hat{\boldsymbol{d}}(t)$, there exist positive constants $c_7$, $c_8$ such that $\|\boldsymbol{g}\| \le c_7\|\boldsymbol{\xi}_a(t)\| + c_8$. Therefore, the inequality in Eq. (64) can be written as

$$\begin{aligned}\dot{V}_2(t) &\le -\lambda_{\min}(Q_a)\|\boldsymbol{\xi}_a(t)\|^2 + 2c_9\|\boldsymbol{n}_r(t)\|\\ &+ 2c_{10}\|\xi_a(t)\|\|\boldsymbol{n}_r(t)\| + 2c_{11}\|\boldsymbol{\xi}_a(t)\|\|\boldsymbol{\delta}(t)\|\end{aligned} \tag{64}$$

where

$$c_9 = 2\left(\frac{\tilde{b}_a^*}{b_T}c_8 + \tilde{d}_a^*\right)\left\|B_a^\top P_a B_a\right\|$$

$c_{11} = \|P_a B_a\|$, and $c_{10} = (\tilde{b}_a^*/b_T)c_7\|B_a^\top P_a B_a\| + \|P_a B_n\|$. Completing the squares in Eq. (64) yields

$$\begin{aligned}\dot{V}_2(t) &\le -k_a\|\boldsymbol{\xi}_a(t)\|^2 + c_{10}^2 c_{12}^2\|\boldsymbol{n}_r(t)\|^2 + c_{11}^2 c_{13}^2\|\boldsymbol{\delta}(t)\|^2\\ &+ 2c_9\|\boldsymbol{n}_r(t)\|\end{aligned} \tag{65}$$

where $c_{12}$, $c_{13}$ are positive constants such that

$$k_a = \lambda_{\min}(Q_a) - \frac{1}{c_{12}^2} - \frac{1}{c_{13}^2} > 0$$

Because $\boldsymbol{\delta}(t) \in \mathcal{L}_\infty$, for any bounded $\boldsymbol{n}_r(t)$ there exists some $\rho_a > 0$ such that $c_{10}^2 c_{12}^2\|\boldsymbol{n}_r(t)\|^2 + c_{11}^2 c_{13}^2\|\delta(t)\|^2 + 2c_9\|\boldsymbol{n}_r(t)\| \le \rho_a$. From the relationship in Eq. (65), it follows that $\dot{V}_2(t) \le 0$ outside the compact set

$$\Omega = \left\{(\boldsymbol{\xi}_a, \tilde{b}, \tilde{\boldsymbol{d}}) : \|\boldsymbol{\xi}_a\| \le \frac{\rho_a}{\sqrt{k_a}}, \|\tilde{b}\| \le \tilde{b}_*, \|\tilde{\boldsymbol{d}}\| \le \tilde{d}_*\right\}$$

Hence all the signals $\boldsymbol{\xi}_a(t), \tilde{b}(t), \tilde{\boldsymbol{d}}(t), \boldsymbol{g}(t)$ in the systems (58–60) are uniformly ultimately bounded. From Eq. (58) it follows that $\dot{\boldsymbol{\xi}}_a(t)$ is bounded as well.

If $\boldsymbol{n}_r(t) = 0$, the inequality in Eq. (65) reduces to

$$\dot{V}_2(t) \le -k_a\|\boldsymbol{\xi}_a(t)\|^2 + c_{11}^2 c_{13}^2\|\boldsymbol{\delta}(t)\|^2 \tag{66}$$

which can be rearranged and integrated to yield

$$k_a\int_0^t \|\boldsymbol{\xi}_a(\tau)\|^2\,\mathrm{d}\tau \le V_2(0) + c_{11}^2 c_{13}^2\int_0^t \|\boldsymbol{\delta}(\tau)\|^2\,\mathrm{d}\tau \tag{67}$$

Because $\boldsymbol{\delta}(t) \in \mathcal{L}_2$, from Eq. (67) we have

$$\lim_{t\to\infty}\int_0^t \|\boldsymbol{\xi}_a(\tau)\|^2\,\mathrm{d}\tau < \infty \tag{68}$$

Thus, $\boldsymbol{\xi}_a(t) \in \mathcal{L}_2(\mathbb{R}^6)\bigcap\mathcal{L}_\infty(\mathbb{R}^6)$. Also, the error dynamics in Eq. (58) imply that $\dot{\boldsymbol{\xi}}_a(t) \in \mathcal{L}_\infty(\mathbb{R}^6)$. Application of Barbalat's lemma [22] ensures that $\boldsymbol{\xi}_a(t) \to 0$ as $t \to \infty$. If the estimated reference command $\hat{\boldsymbol{r}}_{\text{com}}(t)$ is exciting in at least one component, then the application of Lemma 3 will guarantee asymptotic convergence of the parameter errors to zero. The proof is complete. □

To complete the guidance design, we show that the estimator gain matrix $L_f$ can be chosen according to Kalman's scheme (see, for example, [26]). To this end, we write the overall closed-loop error dynamics for the state vector

$$\boldsymbol{\xi}_c = \begin{bmatrix}\boldsymbol{e}^\top & \tilde{\boldsymbol{r}}^\top & \tilde{\boldsymbol{d}}^\top & \tilde{b}\end{bmatrix}^\top \in \mathbb{R}^{10}$$

in the time-varying linear system form:

$$\dot{\boldsymbol{\xi}}_c(t) = A_c(t)\boldsymbol{\xi}_c(t) + B_c\boldsymbol{n}_r(t) + B_\delta\boldsymbol{\delta}(t) \qquad \tilde{\boldsymbol{r}}(t) = C_c\boldsymbol{\xi}_c(t) \tag{69}$$

where

$$A_c(t) = \begin{bmatrix} A_a & -\frac{1}{b_T}B_a & -\frac{1}{b_T}B_a\mathbf{g}(t)\\ G_1(t) & 0_{3\times3} & 0_{3\times1}\\ G_2(t) & 0_{1\times3} & 0\end{bmatrix}, \qquad B_c = \begin{bmatrix}0_{3\times3}\\ -L_f\\ 0_{3\times3}\\ 0_{1\times3}\end{bmatrix}$$

$$C_c = \begin{bmatrix}0_{3\times3}\\ I_{3\times3}\\ 0_{3\times3}\\ 0_{1\times3}\end{bmatrix}^T, \qquad B_\delta = \begin{bmatrix}B_a\\ 0_{3\times3}\\ 0_{1\times3}\end{bmatrix}$$

and $3\times6$ matrix $G_1(t)$ and $1\times6$ matrix $G_2(t)$ are defined through the definition of the projection operator in the adaptive laws in Eq. (60). Their explicit expressions are not presented here. Although the closed-loop error dynamics are nonlinear, the linear form in Eq. (69) can be justified by the fact that all the signals in the systems (58–60) are bounded for all $t \ge 0$ as stated by Theorem 2.

The necessary condition for the estimate $\hat{\boldsymbol{r}}(t)$ to be optimal in the sense of minimizing the performance index $J_n$ in Eq. (56) is that the estimation error must be orthogonal to the measurement data (see, for example, [26], p. 233), that is

$$E\{\tilde{\boldsymbol{r}}(t)\boldsymbol{r}^{*\top}(\tau)\} = 0 \tag{70}$$

for all $\tau \le t$. Then, the estimation error correlation matrix $K_{\tilde{\boldsymbol{r}}}(t,\tau)$ can be computed as follows. Taking into account the orthogonality of the estimator's state for all $\tau \le t$ and the estimation error at time $t$, and the necessary condition in Eq. (70), we write

$$K_{\tilde{r}}(t,\tau) = E\{\tilde{\boldsymbol{r}}(t)\tilde{\boldsymbol{r}}^{\top}(\tau)\} = E\{\tilde{\boldsymbol{r}}(t)[\boldsymbol{r}(\tau) - \hat{\boldsymbol{r}}(\tau)]^{\top}\}$$
$$= E\{\tilde{\boldsymbol{r}}(t)[\boldsymbol{r}^{*}(\tau) - \boldsymbol{n}_r(\tau) - \hat{\boldsymbol{r}}(\tau)]^{\top}\} = -E\{\tilde{\boldsymbol{r}}(t)\boldsymbol{n}_r^{\top}(\tau)\} \tag{71}$$

The output $\tilde{\boldsymbol{r}}(t)$ of the linear system (69) can be written as

$$\tilde{\boldsymbol{r}}(t) = C_c\Phi_c(t,0)\boldsymbol{\xi}_c(0) + C_c\int_0^t \Phi_c(t,s)[B_c\boldsymbol{n}_r(s) + B_\delta\boldsymbol{\delta}(s)]\,\mathrm{d}s$$

where $\Phi_c(t,\tau)$ is the state transition matrix of the system (69). Substituting $\tilde{\boldsymbol{r}}(t)$ from Eq. (72) into Eq. (71), we get

$$K_{\tilde{r}}(t,\tau) = -E\{C_c\Phi_c(t,0)\xi_c(0)\boldsymbol{n}_r^{\top}(\tau)\}$$
$$- E\left\{C_c\int_0^t \Phi_c(t,s)B_c\boldsymbol{n}_r(s)\,\mathrm{d}s\boldsymbol{n}_r^{\top}(\tau)\right\}$$
$$- E\left\{C_c\int_0^t \Phi_c(t,s)B_\delta\boldsymbol{\delta}(s)\,\mathrm{d}s\boldsymbol{n}_r^{\top}(\tau)\right\}$$

Taking into account the zero-mean property of the noise, Eq. (72) reduces to

$$K_{\tilde{r}}(t,\tau) = -C_c\int_0^t \Phi_c(t,s)B_cE\{\boldsymbol{n}_r(s)\boldsymbol{n}_r^{\top}(\tau)\}\,\mathrm{d}s$$
$$= -C_c\int_0^t \Phi_c(t,s)B_cK_{\boldsymbol{n}_r}(s,\tau)\delta(s-\tau)\,\mathrm{d}s$$

Because $\Phi_c(t,t) = \mathbb{I}$ and

$$\int_0^t f(s)\delta(s-t)\,\mathrm{d}s = f(t)$$

for any integrable function $f(t)$, we conclude that

$$K_{\tilde{r}}(t,t) = -C_cB_cK_{\boldsymbol{n}_r}(t,t) = L_f(t)K_{\boldsymbol{n}_r}(t,t) \tag{72}$$

and therefore, the estimator gain matrix can be computed as

$$L_f(t) = K_{\tilde{r}}(t,t)K_{\boldsymbol{n}_r}^{-1}(t,t) \tag{73}$$

It can be verified that the evolution of the estimation error correlation matrix is described by the differential equation (see, for example, [26], p. 71)

$$\dot{K}_{\boldsymbol{\xi}}(t) = A_c(t)K_{\boldsymbol{\xi}}(t) + K_{\boldsymbol{\xi}}(t)A_c^{\top}(t) + B_cK_{\boldsymbol{n}_r}(t)B_c^{\top}$$
$$K_{\tilde{r}}(t) = C_cK_{\boldsymbol{\xi}}(t)C_c^{\top} \tag{74}$$

*Remark 6*. If we assume a constant correlation matrix $K_{\boldsymbol{n}_r}$ for the measurement noise $\boldsymbol{n}_r(t)$, there exists a steady-state estimator gain in two cases: in the case of target interception that is solved without an excitation signal and in the case of formation flight with the constant reference command $\boldsymbol{R}_{\mathrm{com}}$ when the intelligent excitation is used. In these two cases, it can be shown that $A_c(t) \to \bar{A}_c$ as $t \to \infty$, where $\bar{A}_c$ is a constant matrix. Therefore, the steady-state solution can be found according to equations

$$0 = \bar{A}_cK_{\boldsymbol{\xi}} + K_{\boldsymbol{\xi}}\bar{A}_c^{\top} + B_cK_{\boldsymbol{n}_r}B_c^{\top}$$
$$L_f = K_{\tilde{r}}K_{\boldsymbol{n}_r}^{-1} = C_cK_{\boldsymbol{\xi}}C_c^{\top}K_{\boldsymbol{n}_r}^{-1} \tag{75}$$

*Remark 7*. The nonlinear observation model in Eq. (51) can lead to a bias plus a Gaussian noise component. We approximate the nonlinear functions by the first-order Taylor series expansion, like in the extended Kalman filter applications (see, for example, [27]). In this case, in the expression $r^{*}(t) = r(t) + n_r(t)$, the signal $n_r(t) = L_{E/B}\nabla\boldsymbol{f}(y_I(t), z_I(t), b_I(t))n_I(t)$ is a linear function of zero-mean Gaussian noise $n_I(t)$. The neglected terms in the preceding approximation are of higher order in $n_I(t)$ and are small for small values of measurement noise. The zero-mean Gaussian assumption for $n_r(t)$ is not crucial for the stability of the system, because Theorem 2 guarantees bounded tracking errors for any bounded noise process $n_r(t)$, whether it has a bias term or not. However, the error correlation matrix $K_{\tilde{r}}$ and, hence, the filter gain matrix $L_f$, will be affected. The investigation of this effect is not pursued in the paper.

## VI. Inner-Loop Implementation

In this section, we present the implementation of guidance law given in Eqs. (55) and (60) based on the state estimate $\hat{\boldsymbol{r}}(t)$.

### A. Reference Command Formulation

The guidance law $\boldsymbol{V}_F(t)$ in Eq. (55) that guarantees tracking of the maneuvering target subject to Assumption 1, represents the follower's desired inertial velocity vector. The aircraft's actual control surface deflections must be defined to ensure that the aircraft center of gravity at every instant of time has that inertial velocity $\boldsymbol{V}_F(t)$. Because $\boldsymbol{V}_F(t)$ is a smooth function of $t$, we can differentiate it to obtain the inertial acceleration $\boldsymbol{a}_F(t)$ for the center of gravity moving with the velocity $\boldsymbol{V}_F(t)$. Because the analytic differentiation will involve unknown disturbances through the definitions in Eqs. (58) and (60), it can be done numerically using, for example, the technique from [28].

The desired airspeed

$$V_c = \|\boldsymbol{V}_F(t)\| \tag{76}$$

the flight path angle

$$\gamma = -\sin^{-1}\left(\frac{V_{Fx}}{V_c}\right) \tag{77}$$

and the azimuth angle

$$\chi = \tan^{-1}\left(\frac{V_{Fy}}{V_{Fy}}\right) \tag{78}$$

can be straightforwardly computed. Next, we compute the aircraft's desired attitude angles. To this end, recall that the inertial forces acting on the aerial vehicle can be calculated from Newton's second law

$$\boldsymbol{F} = m\boldsymbol{a}_F \tag{79}$$

where $m$ is the aircraft's mass. The inertial force can be transformed into the wind-axis force as follows:

$$\boldsymbol{F}^{W} = L_{W/E}\boldsymbol{F} \tag{80}$$

where $L_{W/E}$ is the coordinate transformation matrix from the inertial frame to the wind frame. It is defined similar to $L_{B/E}$ in Eq. (9) by replacing the body-axis Euler angles $\phi$, $\theta$, $\psi$ by the wind-axis Euler angles $\mu$, $\gamma$, $\chi$. The angles $\gamma$, $\chi$ have been already computed, but the wind-axis roll angle $\mu$ still needs to be determined. Using the wind-axis force components [21], we can write the following equation:

$$\begin{bmatrix} T\cos\alpha\cos\beta - D - mg\sin\gamma \\ -T\cos\alpha\sin\beta - C + mg\sin\mu\cos\gamma \\ -T\sin\alpha - L + mg\cos\mu\cos\gamma \end{bmatrix} = \boldsymbol{F}^{W} \tag{81}$$

where $T$ is the thrust, $D$ is the drag, $C$ is the side force, $L$ is the lift, $\alpha$ is the angle of attack, $\beta$ is the sideslip angle, and $g$ is the gravity acceleration. In these three equations, we have seven unknowns: $T$, $D$, $C$, $L$, $\alpha$, $\beta$, $\mu$. One more equation can be obtained from the condition that all the turns made by the aircraft need to be perfectly coordinated [29], that is, the side force is zero. In this case, we can assume that the sideslip angle can be neglected. Therefore, the second equation in Eq. (81) reduces to

$$mg\sin\mu\cos\gamma = F_y^{W} \tag{82}$$

from which the desired $\mu$ can be computed as follows:

$$\tan\mu = \frac{a_{Fx}\sin\chi - a_{Fy}\cos\chi}{a_{Fx}\sin\gamma\cos\chi + a_{Fy}\sin\gamma\sin\chi + (a_{Fz}-g)\cos\gamma}$$

Neglecting $\beta$ in the remaining two equations in Eq. (81) reduces them to

$$\begin{aligned} T\cos\alpha - D - mg\sin\gamma &= F_x^W \\ -T\sin\alpha - L + mg\cos\mu\cos\gamma &= F_z^W \end{aligned} \tag{83}$$

where $F_x^W$ and $F_z^W$ are the wind-axis force components that are now available. Here, we recall that the control surface deflections are primarily moment generators for the conventional aircraft with no direct force control; therefore, the dependence of the lift and drag forces on these deflections can be neglected: $C_D = C_D(\alpha)$, $C_L = C_L(\alpha, \dot{\alpha}, q)$, where $C_D = (D/\bar{q}S)$ and $C_L = L/(\bar{q}S)$ are, respectively, the drag and lift coefficients, $\bar{q} = \frac{1}{2}\rho V_c^2$ is the dynamic pressure, $\rho$ is the air density, and $q$ is the pitch rate. The presence of $q$ in the lift coefficient requires differentiation of wind-axis Euler angles and can be done numerically as it is done in Eq. [28]. In that case, solving the two equations in Eq. (83) will result in a differential equation for $\alpha$. Here, we make a simplifying assumption that the lift dependence on the angle-of-attack rate and pitch rate is negligible so that $C_L = C_L(\alpha) = C_{LO} + C_{L\alpha}\alpha$. The drag force can be expressed using the parabolic drag polar equation $C_D = C_{D0} + KC_L^2$. From the equations in Eq. (83), we can easily derive the following equation to be solved for $\alpha$:

$$\begin{aligned} -D\sin\alpha - L\cos\alpha &= \left(F_x^W + mg\sin\gamma\right)\sin\alpha \\ &+ (F_z^W - mg\cos\mu\cos\gamma)\cos\alpha \end{aligned} \tag{84}$$

With $\beta = 0$, the transformation matrix $L_{B/W}$ from the wind to body axis reduces to

$$L_{B/W} = \begin{bmatrix} \cos\alpha & 0 & -\sin\alpha \\ 0 & 1 & 0 \\ \sin\alpha & 0 & \cos\alpha \end{bmatrix} \tag{85}$$

Using the relationship $L_{B/E} = L_{B/W}L_{W/E}$, the body-axis desired Euler angles can be computed as follows:

$$\begin{aligned} \phi_c = \tan^{-1}\left(\frac{L_{B/E}(2,3)}{L_{B/E}(3,3)}\right) \qquad \theta_c = -\sin^{-1}[L_{B/E}(1,3)] \\ \psi_c = \tan^{-1}\left(\frac{L_{B/E}(1,2)}{L_{B/E}(1,1)}\right) \end{aligned} \tag{86}$$

where $L_{B/E}(i,j)$ denotes the $(i,j)$th entry of the matrix $L_{B/E}$.

*Remark 8.* We can avoid the differentiation of the guidance command $\boldsymbol{V}_F(t)$ by assuming that it represents the inertial velocity of the model that moves with zero sideslip and zero angle of attack, that is, the longitudinal axis of the body (stability) frame of the model is aligned with the inertial velocity vector $\boldsymbol{V}_F(t)$ all the time. In this case

$$\theta_c = \gamma_c = -\sin^{-1}\left(\frac{V_{Fx}^E}{V_c}\right) \tag{87}$$

and

$$\psi_c = \chi_c = \tan^{-1}\left(\frac{V_{Fy}^E}{V_{Fy}^E}\right) \tag{88}$$

and the aircraft is required to track the reference commands $V_c$, $\theta_c$, $\psi_c$. Because there are four control inputs to be selected, we can also satisfy an additional performance specification. For example, we can require the aircraft turns to be perfectly coordinated. This requirement imposes a constraint on the roll angle ([29], p. 190) that can be used to specify the roll reference command:

$$\phi_c = tan^{-1}\left(\Im\frac{\dot{\psi}V}{g}\frac{\cos\beta}{\cos\alpha}\right) \tag{89}$$

where

$$\Im = \frac{(a-b^2) + b\tan\alpha + \sqrt{c(1-b^2) + (\dot{\psi}V)^2\sin^2\beta/g^2}}{a^2 - b^2(1 + c\tan^2\alpha)}$$

$V$ is the airspeed, $a = 1 - (\dot{\psi}V/g)\tan\alpha\sin\beta$, $b = \sin\gamma/\cos\beta$, and $c = 1 + (\dot{\psi}V/g)^2\cos^2\beta$. This approach is incorporated in the simulation example. □

### B. Aircraft Model

Consider the dynamic equations of the aircraft written in combined wind and body axis [29]:

$$\begin{aligned} \dot{V}(t) &= \frac{1}{m}[-D - mg\sin\gamma(t) + T\cos\beta(t)\cos\alpha(t)] \\ \dot{\alpha}(t) &= q(t) - p(t)\cos\alpha(t)\tan\beta(t) - r(t)\sin\alpha(t)\tan\beta(t) \\ &\quad - q_w(t)\sec\beta(t) \\ \dot{\beta}(t) &= r_w(t) + p(t)\sin\alpha(t) - r(t)\cos\alpha(t) \\ \begin{bmatrix} \dot{\phi} \\ \dot{\theta} \\ \dot{\psi} \end{bmatrix} &= P(t)\begin{bmatrix} p(t) \\ q(t) \\ r(t) \end{bmatrix} \\ J\begin{bmatrix} \dot{p}(t) \\ \dot{q}(t) \\ \dot{r}(t) \end{bmatrix} &= -\begin{bmatrix} p(t) \\ q(t) \\ r(t) \end{bmatrix} \times J\begin{bmatrix} p(t) \\ q(t) \\ r(t) \end{bmatrix} + \begin{bmatrix} \mathcal{L} \\ \mathcal{M} \\ \mathcal{N} \end{bmatrix} \end{aligned} \tag{90}$$

with

$$\begin{aligned} P(t) &= \begin{bmatrix} 1 & \sin\phi(t)\tan\theta(t) & \cos\phi(t)\tan\theta(t) \\ 0 & \cos\phi(t) & -\sin\phi(t) \\ 0 & \sin\phi(t)\sec\theta(t) & \cos\phi(t)\sec\theta(t) \end{bmatrix} \\ r_w &= \frac{1}{mV}[-C + mg\sin\mu\cos\gamma - T\sin\beta\cos\alpha] \\ q_w &= \frac{1}{mV}[L - mg\cos\mu\cos\gamma + T\sin\alpha] \\ J &= \begin{bmatrix} J_{xx} & 0 & -J_{xz} \\ 0 & J_{yy} & 0 \\ -J_{xz} & 0 & J_{zz} \end{bmatrix} \end{aligned} \tag{91}$$

where $p$ is the roll rate, $r$ is the yaw rate, and $J$ is the follower's inertia matrix. The body-axis moments are expressed in the form $\mathcal{L} = \mathcal{L}_n + \mathcal{L}_T + \Delta_l$, $\mathcal{M} = \mathcal{M}_n + \mathcal{M}_T + \Delta_m$, $\mathcal{N} = \mathcal{N}_n + \mathcal{N}_T + \Delta_n$, where $\mathcal{L}_n$, $\mathcal{M}_n$, $\mathcal{N}_n$ are respective nominal aerodynamic moments that are known and affine in control surface deflections, $\mathcal{L}_T$,$\mathcal{M}_T$, $\mathcal{N}_T$ are body-axis moments due to engine thrust, and $\Delta_l$, $\Delta_m$, $\Delta_n$ represent uncertainties in the aerodynamic moments not accounted for in the nominal moments. They are associated with the modeling of the aircraft dynamics and the turbulent effect of the closed coupled formation flight due to the tracking of the target. In general, these are unknown functions of states $\boldsymbol{\xi} = \begin{bmatrix} V & \alpha & \beta & p & q & r \end{bmatrix}^\top$ of the system (90) and control $\boldsymbol{u} = \begin{bmatrix} \delta_T & \delta_a & \delta_e & \delta_r \end{bmatrix}^\top$: $\Delta_l(\xi, \boldsymbol{u})$, $\Delta_m(\xi, \boldsymbol{u})$, $\Delta_n(\xi, \boldsymbol{u})$. The aerodynamic forces $D$, $C$, $L$ also are assumed to have nominal known parts $D_n$, $C_n$, $L_n$, and unknown parts $\Delta_D(\xi, \boldsymbol{u})$, $\Delta_C(\xi, \boldsymbol{u})$, $\Delta_L(\xi, \boldsymbol{u})$. The control algorithm presented next will compensate for the uncertainties in the aerodynamic drag force and the aerodynamic moments that are assumed to be bounded and continuous functions of $\boldsymbol{\xi}, \boldsymbol{u} \in \mathcal{D}$, where $\mathcal{D}$ is a compact set of respective possible initial conditions. For these unknown functions, we will use linear in parameters approximations by neural networks with RBFs in their hidden layers [30]:

$$\frac{1}{m}\Delta_D(\boldsymbol{\xi},\boldsymbol{u}) = \boldsymbol{W}_D^\top \boldsymbol{\Phi}(\boldsymbol{\xi},\boldsymbol{u}) + \epsilon_D(\boldsymbol{\xi},\boldsymbol{u})$$
$$J^{-1}\begin{bmatrix}\Delta_l(\boldsymbol{\xi},\boldsymbol{u})\\ \Delta_m(\boldsymbol{\xi},\boldsymbol{u})\\ \Delta_n(\boldsymbol{\xi},\boldsymbol{u})\end{bmatrix} = \begin{bmatrix}\boldsymbol{W}_l^\top \boldsymbol{\Phi}(\boldsymbol{\xi},\boldsymbol{u}) + \epsilon_l(\boldsymbol{\xi},\boldsymbol{u})\\ \boldsymbol{W}_m^\top \boldsymbol{\Phi}(\boldsymbol{\xi},\boldsymbol{u}) + \epsilon_m(\boldsymbol{\xi},\boldsymbol{u})\\ \boldsymbol{W}_n^\top \boldsymbol{\Phi}(\boldsymbol{\xi},\boldsymbol{u}) + \epsilon_n(\boldsymbol{\xi},\boldsymbol{u})\end{bmatrix} \tag{92}$$
$$\|\epsilon_D(\boldsymbol{\xi},\boldsymbol{u})\| \le \epsilon_D^*, \qquad \|\epsilon_l(\boldsymbol{\xi},\boldsymbol{u})\| \le \epsilon_l^*$$
$$\|\epsilon_m(\boldsymbol{\xi},\boldsymbol{u})\| \le \epsilon_m^*, \qquad \|\epsilon_n(\boldsymbol{\xi},\boldsymbol{u})\| \le \epsilon_n^*$$

where $\boldsymbol{W}_i \in \mathbb{R}^{N_i}$, $i = D, l, m, n$, are the vectors of unknown constant parameters and $\boldsymbol{\Phi}(\boldsymbol{\xi},\boldsymbol{u})$ is the vector of RBFs. Also, we assume that the thrust and nominal aerodynamic moments can be represented as follows

$$T = \frac{1}{2}\rho V_F^2 S C_{T_{\delta_T}}\delta_T$$
$$\mathcal{L}_n = \frac{1}{2}\rho V_F^2 S b[C_l(\beta,p,r) + C_{l_{\delta_a}}\delta_a + C_{l_{\delta_r}}\delta_r]$$
$$\mathcal{N}_n = \frac{1}{2}\rho V_F^2 S b[C_n(\beta,p,r) + C_{n_{\delta_a}}\delta_a + C_{n_{\delta_r}}\delta_r] \tag{93}$$
$$\mathcal{M}_n = \frac{1}{2}\rho V_F^2 S \bar{c}[C_m(M,\alpha,q) + C_{m_{\delta_e}}\delta_e]$$

Here, $S$ is the aircraft's reference area, $b_F$ is the follower's wing span, $\bar{c}$ is the mean-aerodynamic chord, $C_{T_{\delta T}}, C_{l_{\delta_a}}, C_{l_{\delta_r}}, C_{n_{\delta_a}}, C_{n_{\delta_r}}, C_{m_{\delta_e}}$ are the corresponding control effectiveness, and $C_l$, $C_n$, $C_m$ are the aerodynamic coefficients.

### C. Control Design

In this section, we derive the control surface deflection commands $\boldsymbol{u} = \begin{bmatrix}\delta_T & \delta_e & \delta_a & \delta_r\end{bmatrix}^\top$ to track the desired motion. Because there are four control inputs, we chose $V, \phi, \theta, \psi$ as the regulated outputs to track the desired velocity and attitude commands $V_c$, $\phi_c$, $\theta_c$, $\psi_c$ in Eqs. (76–78) and (83). For this purpose, we first derive desired laws for $T, \mathcal{L}_n, \mathcal{M}_n, \mathcal{N}_n$ for the dynamics in Eq. (90) to track the reference commands $[V_c(t), \phi_c(t), \theta_c(t), \psi_c(t)]$. These can be inverted afterward to obtain the actual throttle and control surface deflections using the relationships in Eq. (93).

#### 1. Velocity Control

We start with the first equation in Eq. (90) to design the tracking control law for the velocity command $V_c(t)$ and set

$$T(t) = \frac{1}{\cos\alpha(t)\cos\beta(t)} g\sin\gamma(t) + D^n(\boldsymbol{\xi}(t),\boldsymbol{u}(t)) + m[\hat{\boldsymbol{W}}_D^\top(t)\boldsymbol{\Phi}(\boldsymbol{\xi}(t),\boldsymbol{u}(t)) - k_V(V(t) - V_c(t)) + \dot{V}_c(t)] \tag{94}$$

where $k_V > 0$ is the desired time constant (design parameter), and $\hat{\boldsymbol{W}}_D(t)$ is the estimate of the unknown weight vector $\boldsymbol{W}_D$, which is updated online. Defining the tracking error as $e_V = V(t) - V_c(t)$, the error dynamics can be written as

$$\dot{e}_V(t) = -k_V e_V(t) - \tilde{\boldsymbol{W}}_D^\top(t)\Phi(\xi(t),\boldsymbol{u}(t)) - \epsilon_D(\xi(t),\boldsymbol{u}(t)) \tag{95}$$

where $\tilde{\boldsymbol{W}}_D(t) = \hat{\boldsymbol{W}}_D(t) - \boldsymbol{W}_D$ is the parameter error. The adaptive law for the estimate $\hat{\boldsymbol{W}}_D(t)$ is designed using the following Lyapunov function candidate

$$V_3(e_V, \tilde{\boldsymbol{W}}_D) = \frac{1}{2}e_V^2(t) + \tilde{\boldsymbol{W}}_D^\top(t) G_D^{-1}\tilde{\boldsymbol{W}}_D(t) \tag{96}$$

where $G_D > 0$ is the adaptive gain. It is straightforward to verify that the derivative of $V_3$ along the trajectory of the system (95) satisfies the inequality

$$\dot{V}_3(t) \le -k_V e_V^2(t) - e_V(t)\epsilon_D(\boldsymbol{\xi}(t),\boldsymbol{u}(t)) \tag{97}$$

if we set

$$\dot{\hat{\boldsymbol{W}}}_D(t) = G_D \mathrm{Proj}(\hat{\boldsymbol{W}}_D(t), e_V(t)\boldsymbol{\Phi}(\boldsymbol{\xi}(t),\boldsymbol{u}(t))) \tag{98}$$

where the projection operator $\mathrm{Proj}(\cdot,\cdot)$ guarantees boundedness of the estimate $\hat{\boldsymbol{W}}_D(t)$ and, hence, the parameter error $\tilde{\boldsymbol{W}}_D(t)$. The inequality (97) implies that the tracking error is uniformly ultimately bounded.

#### 2. Orientation Control

Next, we use the block-backstepping technique from [31] to design the pseudo controls $p_c(t)$, $q_c(t)$, $r_c(t)$ for the Euler angles dynamic equations to track the reference commands $\phi_c(t)$, $\theta_c(t)$, $\psi_c(t)$. To this end, we set

$$\begin{bmatrix}p_c(t)\\ q_c(t)\\ r_c(t)\end{bmatrix} = H(t)\begin{bmatrix}-k_\phi[\phi(t) - \phi_c(t)] + \dot{\phi}_c(t)\\ -k_\theta[\theta(t) - \theta_c(t)] + \dot{\theta}_c(t)\\ -k_\psi[\psi(t) - \psi_c(t)] + \dot{\psi}_c(t)\end{bmatrix}$$

where $k_\phi > 0$, $k_\theta > 0$, $k_\psi > 0$ are the desired time constants (design parameters), whereas

$$H(t) = \begin{bmatrix}1 & 0 & -\sin\theta(t)\\ 0 & \cos\phi(t) & \sin\phi(t)\cos\theta(t)\\ 0 & -\sin\phi(t) & \cos\phi(t)\cos\theta(t)\end{bmatrix}$$

Then, defining the tracking errors as $e_\phi(t) = \phi(t) - \phi_c(t)$, $e_\theta(t) = \theta(t) - \theta_c(t)$, and $e_\psi(t) = \psi(t) - \psi_c(t)$, the corresponding error dynamics result in the system

$$\dot{e}_\phi(t) = -k_\phi e_\phi(t)$$
$$\dot{e}_\theta(t) = -k_\theta e_\theta(t)$$
$$\dot{e}_\psi(t) = -k_\psi e_\psi(t) \tag{99}$$

which is exponentially stable. Therefore, denoting the corresponding errors by $e_p(t) = p(t) - p_c(t)$, $e_q(t) = q(t) - q_c(t)$, and $e_r(t) = r(t) - r_c(t)$, and designing the nominal aerodynamic moments as

$$\begin{bmatrix}\mathcal{L}_n(t)\\ \mathcal{M}_n(t)\\ \mathcal{N}_n(t)\end{bmatrix} = \begin{bmatrix}p(t)\\ q(t)\\ r(t)\end{bmatrix}\times J\begin{bmatrix}p(t)\\ q(t)\\ r(t)\end{bmatrix} - JP(t)\begin{bmatrix}e_\phi(t)\\ e_\theta(t)\\ e_\psi(t)\end{bmatrix} - J\begin{bmatrix}\hat{\boldsymbol{W}}_l(t)^\top\boldsymbol{\Phi}(\boldsymbol{\xi},\boldsymbol{u})\\ \hat{\boldsymbol{W}}_m(t)^\top\boldsymbol{\Phi}(\boldsymbol{\xi},\boldsymbol{u})\\ \hat{\boldsymbol{W}}_n(t)^\top\boldsymbol{\Phi}(\boldsymbol{\xi},\boldsymbol{u})\end{bmatrix} + J\begin{bmatrix}-k_p e_p(t) + \dot{p}_c(t)\\ -k_q e_q(t) + \dot{q}_c(t)\\ -k_r e_r(t) + \dot{r}_c(t)\end{bmatrix} \tag{100}$$

where $k_p > 0$, $k_r > 0$, $k_q > 0$ are the desired time constants (design parameters) and $\hat{\boldsymbol{W}}_l(t)$, $\hat{\boldsymbol{W}}_m(t)$, $\hat{\boldsymbol{W}}_n(t)$ are, respectively, the estimates of the unknown weight vectors $\boldsymbol{W}_l, \boldsymbol{W}_m, \boldsymbol{W}_n$ that are updated online, the overall error dynamics can be written as follows

$$\begin{bmatrix}\dot{e}_\phi(t)\\ \dot{e}_\theta(t)\\ \dot{e}_\psi(t)\end{bmatrix} = \begin{bmatrix}-k_\phi e_\phi(t)\\ -k_\theta e_\theta(t)\\ -k_\psi e_\psi(t)\end{bmatrix} + P(t)\begin{bmatrix}e_p(t)\\ e_q(t)\\ e_r(t)\end{bmatrix}$$
$$\begin{bmatrix}\dot{e}_p(t)\\ \dot{e}_q(t)\\ \dot{e}_r(t)\end{bmatrix} = \begin{bmatrix}-k_p e_p(t)\\ -k_q e_q(t)\\ -k_r e_r(t)\end{bmatrix} - P(t)\begin{bmatrix}e_\phi(t)\\ e_\theta(t)\\ e_\psi(t)\end{bmatrix} - \begin{bmatrix}\tilde{\boldsymbol{W}}_l^\top(t)\boldsymbol{\Phi}(\xi(t),\boldsymbol{u}(t)) - \epsilon_l(\xi(t),\boldsymbol{u}(t))\\ \tilde{\boldsymbol{W}}_m^\top(t)\boldsymbol{\Phi}(\xi(t),\boldsymbol{u}(t)) - \epsilon_m(\xi(t),\boldsymbol{u}(t))\\ \tilde{\boldsymbol{W}}_n^\top(t)\boldsymbol{\Phi}(\xi(t),\boldsymbol{u}(t)) - \epsilon_n(\xi(t),\boldsymbol{u}(t))\end{bmatrix} \tag{101}$$

where $\tilde{\boldsymbol{W}}_l(t) = \hat{\boldsymbol{W}}_l(t) - \boldsymbol{W}_l$, $\tilde{\boldsymbol{W}}_m(t) = \hat{\boldsymbol{W}}_m(t) - \boldsymbol{W}_m$, and $\tilde{\boldsymbol{W}}_n(t) = \hat{\boldsymbol{W}}_n(t) - \boldsymbol{W}_n$ are the parameter estimation errors.

Consider the following Lyapunov function candidate for the error dynamics in Eq. (101):

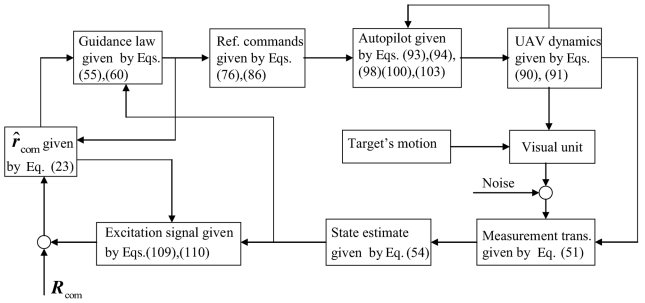


**Fig. 3 Control system schematics.**

$$V_4(e_\phi, e_\theta, e_\psi, e_p, e_q, e_r, \tilde{\boldsymbol{W}}_l, \tilde{\boldsymbol{W}}_m, \tilde{\boldsymbol{W}}_n) = \frac{1}{2}e_\phi^2(t) + \frac{1}{2}e_\theta^2(t) + \frac{1}{2}e_\psi^2(t) + \frac{1}{2}e_p^2(t) + \frac{1}{2}e_q^2(t) + \frac{1}{2}e_r^2(t) + \tilde{\boldsymbol{W}}_l^\top(t)G_p^{-1}\tilde{\boldsymbol{W}}_l(t) + \tilde{\boldsymbol{W}}_m^\top(t)G_q^{-1}\tilde{\boldsymbol{W}}_m(t) + \tilde{\boldsymbol{W}}_n^\top(t)G_r^{-1}\tilde{\boldsymbol{W}}_n(t) \tag{102}$$

where $G_l > 0$, $G_m > 0$, $G_n > 0$ are the adaptive gains. If we define the adaptive laws for the estimates $\hat{\boldsymbol{W}}_l(t)$, $\hat{\boldsymbol{W}}_m(t)$, and $\hat{\boldsymbol{W}}_n(t)$ as

$$\begin{aligned}\dot{\hat{\boldsymbol{W}}}_l(t) &= G_p\text{Proj}(\hat{\boldsymbol{W}}_l(t), e_p(t)\boldsymbol{\Phi}(\boldsymbol{\xi}(t), \boldsymbol{u}(t)))\\ \dot{\hat{\boldsymbol{W}}}_m(t) &= G_q\text{Proj}(\hat{\boldsymbol{W}}_m(t), e_q(t)\boldsymbol{\Phi}(\boldsymbol{\xi}(t), \boldsymbol{u}(t)))\\ \dot{\hat{\boldsymbol{W}}}_n(t) &= G_r\text{Proj}(\hat{\boldsymbol{W}}_n(t), e_r(t)\boldsymbol{\Phi}(\boldsymbol{\xi}(t), \boldsymbol{u}(t)))\end{aligned} \tag{103}$$

then it can be verified that

$$\dot{V}_4(t) \le -k_\phi e_\phi^2(t) - k_\theta e_\theta^2(t) - k_\psi e_\psi^2(t) - k_p e_p^2(t) - e_p(t)\epsilon_l(\boldsymbol{\xi}(t), \boldsymbol{u}(t)) - k_q e_q^2(t) - e_q(t)\epsilon_m(\boldsymbol{\xi}(t), \boldsymbol{u}(t)) - k_r e_r^2(t) - e_r(t)\epsilon_n(\boldsymbol{\xi}(t), \boldsymbol{u}(t)) \tag{104}$$

Taking into account the uniform bounds on the function approximation errors in Eq. (92), the following upper bound can be written

$$\dot{V}_4(t) \le -k_\phi e_\phi^2(t) - k_\theta e_\theta^2(t) - k_\psi e_\psi^2(t) - |e_p(t)|(k_p|e_p(t)| - \epsilon_l^*) - |e_q(t)|(k_q|e_q(t)| - \epsilon_m^*) - |e_r(t)|(k_r|e_r(t)| - \epsilon_n^*) \tag{105}$$

It follows that $\dot{V}_4 \le 0$ outside the compact region

$$\Omega = \{|e_p(t)| \le k_p^{-1}\epsilon_l^*, |e_q(t)| \le k_q^{-1}\epsilon_m^*, |e_r(t)| \le k_r^{-1}\epsilon_n^*, \| \tilde{\boldsymbol{W}}_i(t) \| \le W_i^*,\ i = l, m, n\} \tag{106}$$

where the bounds $W_i^*$ are guaranteed by the projection operator used in the adaptive laws in Eq. (103).

The throttle and control surface deflections are easily found by solving the Eqs. (94) and (100) for $\delta_T, \delta_a, \delta_e, \delta_r$, because the nominal aerodynamic moments are assumed to have linear representations in stability derivatives. The implementation architecture is schematically displayed in Fig. 3. The derivation of the control laws is summarized in the following theorem.

*Theorem 3*. The aircraft thrust and the aerodynamic moments defined in Eqs. (94) and (100) along with the adaptive laws in Eqs. (98) and (103) guarantee tracking of the reference commands $V_c(t)$, $\phi_c(t)$, $\theta_c(t)$, $\psi_c(t)$ with uniformly ultimately bounded errors.

If the approximation errors are zero, i.e., $\epsilon_i(x) = 0$, $i = D, l, m, n$, then it follows from Eqs. (97) and (105) that for all $\boldsymbol{\xi}(t)$, $\dot{V}_3(t) \le 0$ and $\dot{V}_4(t) \le 0$. Using Barbalat's lemma, one can show that the tracking error converges to zero asymptotically.

*Remark 9*. The control laws in Eqs. (94) and (100) contain the derivatives of the reference commands $V_c(t)$, $\phi_c(t)$, $\theta_c(t)$, $\psi_c(t)$ that involve unknown disturbance $\boldsymbol{d}(t)$ through the guidance law in Eq. (55). One can prefilter the reference commands $V_c(t)$, $\phi_c(t)$, $\theta_c(t)$, $\psi_c(t)$ by a stable low-pass filter. For instance, for the $V(t)$ dynamics, one can set

$$\dot{V}_m(t) = -\lambda_V[V_m(t) - V_c(t)] \tag{107}$$

where $\lambda_V > 0$ is a constant. In the control law in Eq. (94) one can use $V_m(t)$ instead of $V_c(t)$, and replace the derivative $\dot{V}_m(t)$ by the right-hand side of Eq. (107). To remove the steady-state error, one can define the integral error

$$V_I(t) = \int_0^t V_m(\tau) - V_c(\tau)$$

and write the extended dynamics

$$\begin{aligned}\dot{V}_I(t) &= V_m(t) - V_c(t)\\ \dot{V}_m(t) &= -2\zeta_u\omega_V[V_m(t) - V_c(t)] - \omega_V^2 V_I\end{aligned} \tag{108}$$

where $\zeta_V$, $\omega_V$ are the desired damping ratio and frequency (design parameters). Again, the command $V_c(t)$ can be replaced by $V_m(t)$ in the control law in Eq. (94), its derivative being calculated according to the dynamics in Eq. (108).

## VII. Simulation

The proposed algorithm is simulated for a small UAV model with the following parameters: $m = 0.6293$ slugs, $J = [0.1230\ \ 0\ \ 0; 0\ \ 0.1747\ \ 0; 0\ \ 0\ \ 0.2553]$slugs.ft$^2$, $S = 11.5$ ft$^2$, $c = 1.2547$ ft, $b_F = 9.1$ ft. For the target model, a UAV is chosen with a wing span (maximal size) of 8 ft. The target starts motion from the straight level flight with the velocity of $\boldsymbol{V}_T(0) = \begin{bmatrix}50 & 0 & 0\end{bmatrix}^\top$ ft/s from the position $\boldsymbol{R}_T(0) = \begin{bmatrix}200 & 30 & -20\end{bmatrix}^\top$ ft, where the origin of the inertial frame is placed in the follower's initial position. It makes turning, climbing, diving, and linearly accelerating maneuvers on the first 117 s with the speed ranging from 35 to 60 ft/s. Then it maintains a constant velocity $\boldsymbol{V}_T = \begin{bmatrix}0 & -50 & 0\end{bmatrix}^\top$ ft/s. The target's maneuvers satisfy $\mathcal{L}_2$ requirement, because they take place on finite time interval. The follower is initially in straight level flight with the initial velocity $\boldsymbol{V}_F(0) = \begin{bmatrix}50 & 0 & 0\end{bmatrix}^\top$ ft/s and is commanded to maintain the relative coordinates $\boldsymbol{R}_{\text{com}} = \begin{bmatrix}32 & 8 & 0\end{bmatrix}^\top$ ft. The initial estimation of $b_T$ is set to $\hat{b}(0) = 5$ ft and the initial estimation of $\boldsymbol{d}$ is set to $\hat{\boldsymbol{d}}(0) = \boldsymbol{V}_F(0)/\hat{b}(0)$. The excitation signal is added to the $R_{cy}$ coordinate according to [12] with the following amplitude:

$$a(t) = \begin{cases} k_1, & t \in [0, T)\\ \min\left\{k_2 \int_{t-T}^t \|\mathbf{e}(\tau)\|^2\, \mathrm{d}\tau, k_1 - k_3\right\} + k_3, & t \ge T\end{cases} \tag{109}$$

where $T = 2\pi/\omega$ is the period of the excitation signal

$$s_E = a(t)\sin(\omega t) \tag{110}$$

$k_i > 0$, $i = 1, 2, 3$ are design constants set to $T = 3$ s, $k_1 = 0.4$, $k_2 = 500$, $k_3 = 0$. In general, $k_3$ should be a small positive number, but in the case of measurement noise there is always enough excitation, and so it can be set to zero.

In simulations, no camera model is used. Instead, the tracking error is formed according to the equation

$$\boldsymbol{e}(t) = \frac{1}{b_T}[\boldsymbol{R}_T(t) - \boldsymbol{R}_F(t)] - \hat{\boldsymbol{r}}_{\text{com}}(t) + \boldsymbol{n}_r(t) \tag{111}$$

where $\boldsymbol{n}_r(t)$ is a Gaussian white noise with $SNR = 50$ in all components. The initial conditions for the estimator are set equal to $\hat{\boldsymbol{r}}(0) = \boldsymbol{r}(0) = (1/b_T)[\boldsymbol{R}_T(0) - \boldsymbol{R}_F(0)]$. A prefilter is used for the command shaping with the poles of $-0.2$ and with the initial

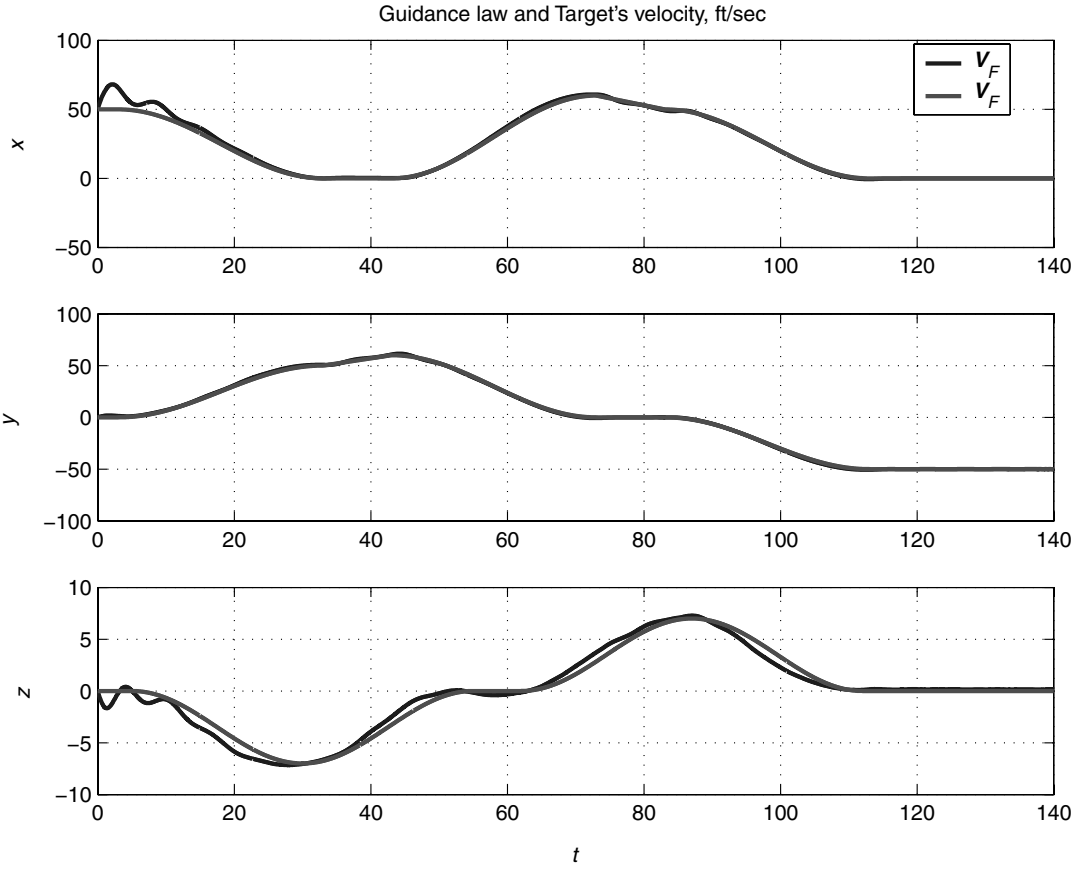


**Fig. 4 Guidance law vs Target's inertial velocity.**

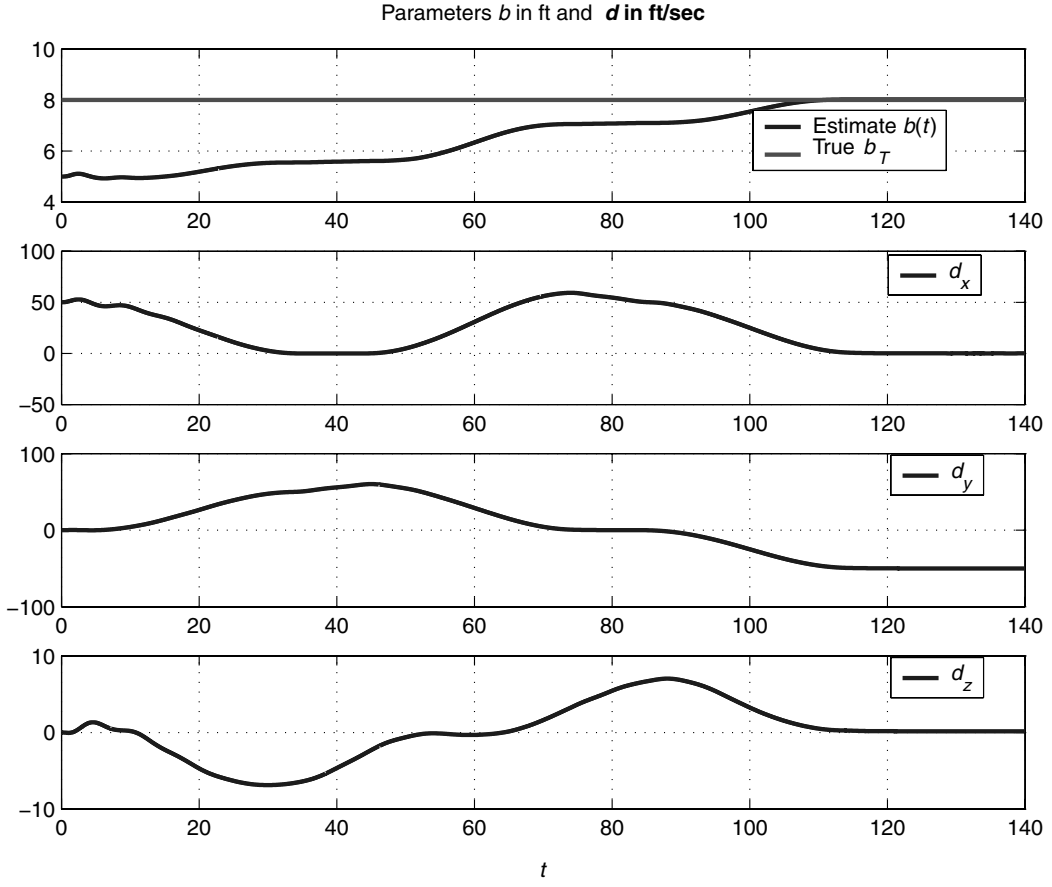


**Fig. 5 Parameter convergence.**

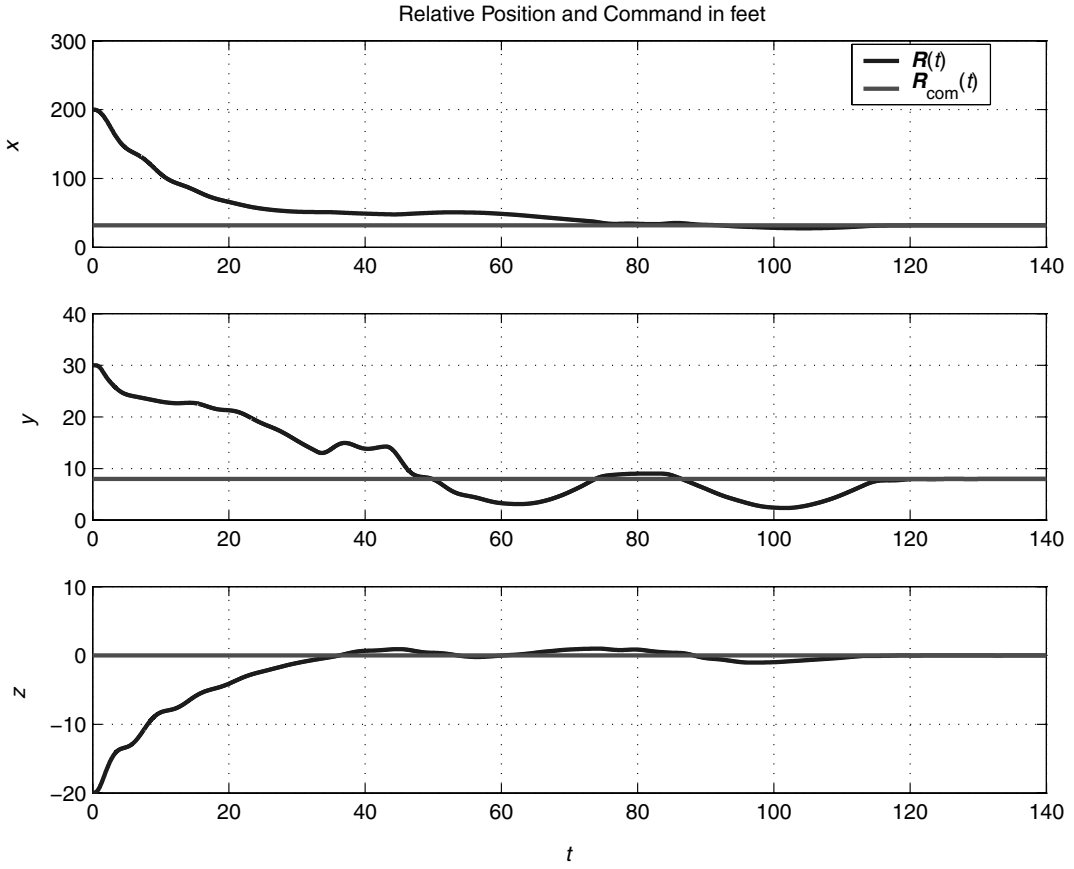


**Fig. 6 Target's and follower's relative position.**

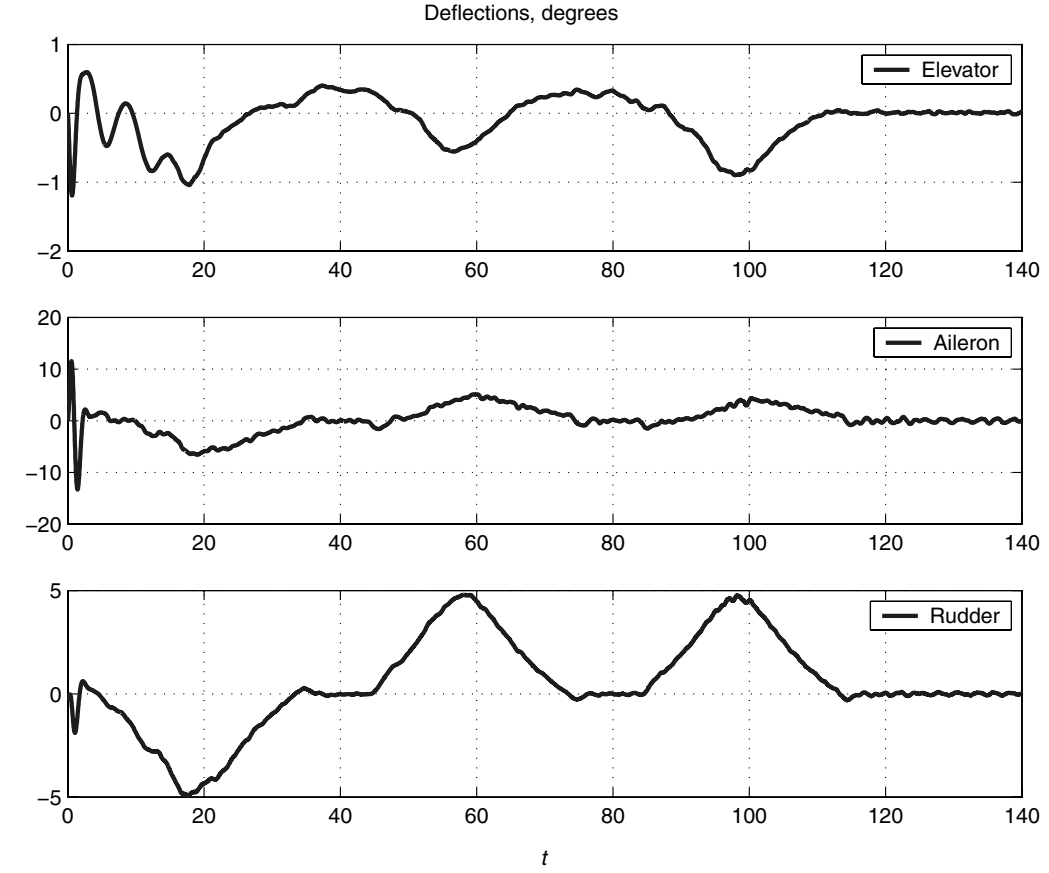


**Fig. 7 Control surface deflections.**

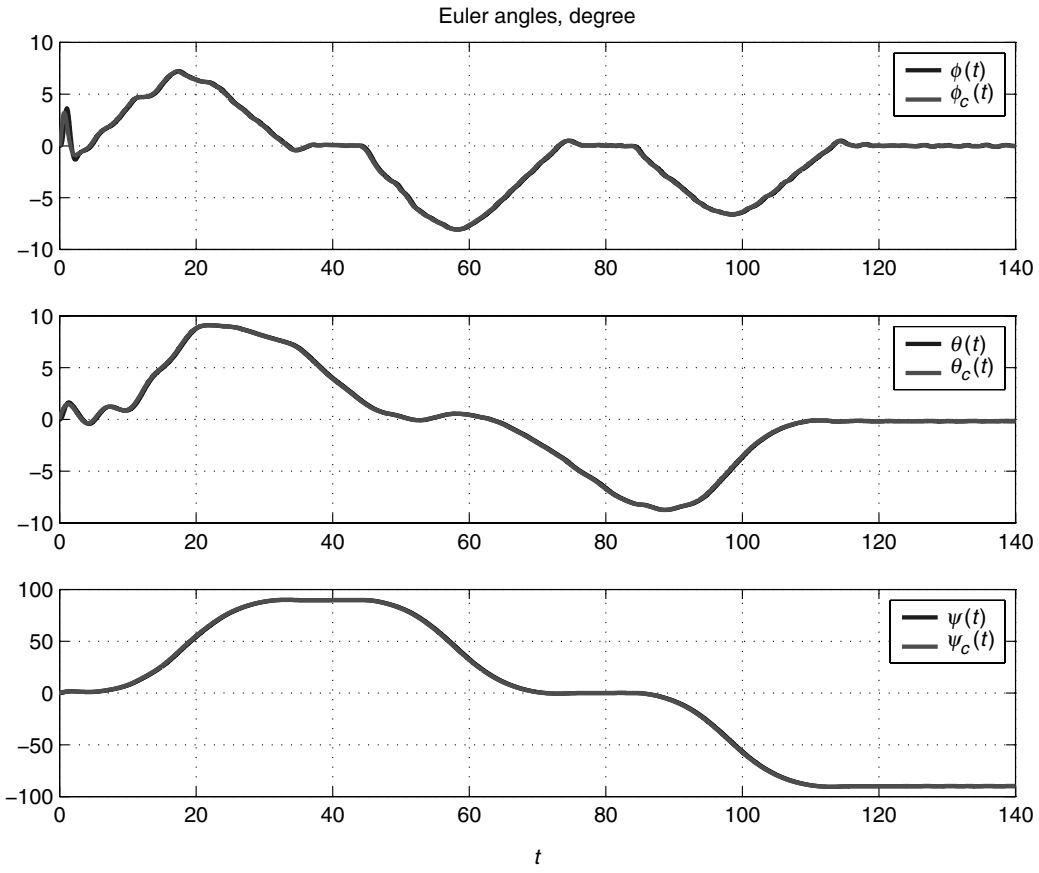


**Fig. 8 Euler angles responses.**

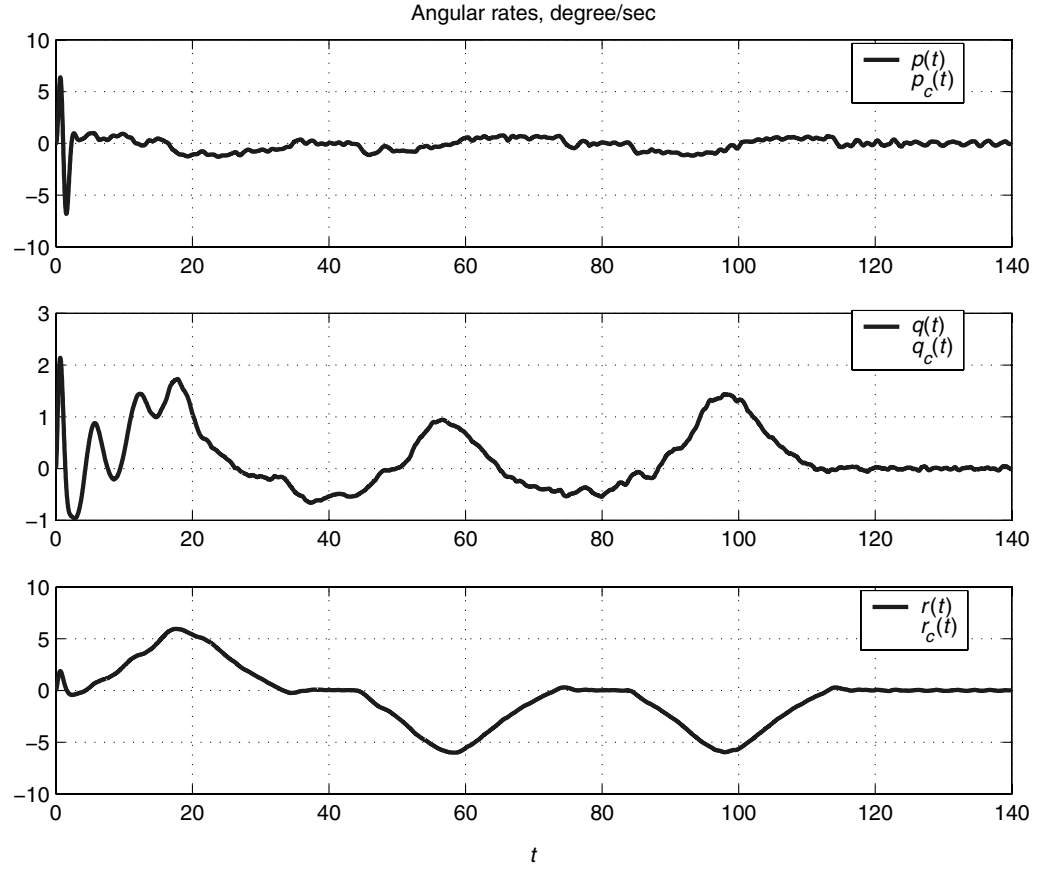


**Fig. 9 Angular rates responses.**

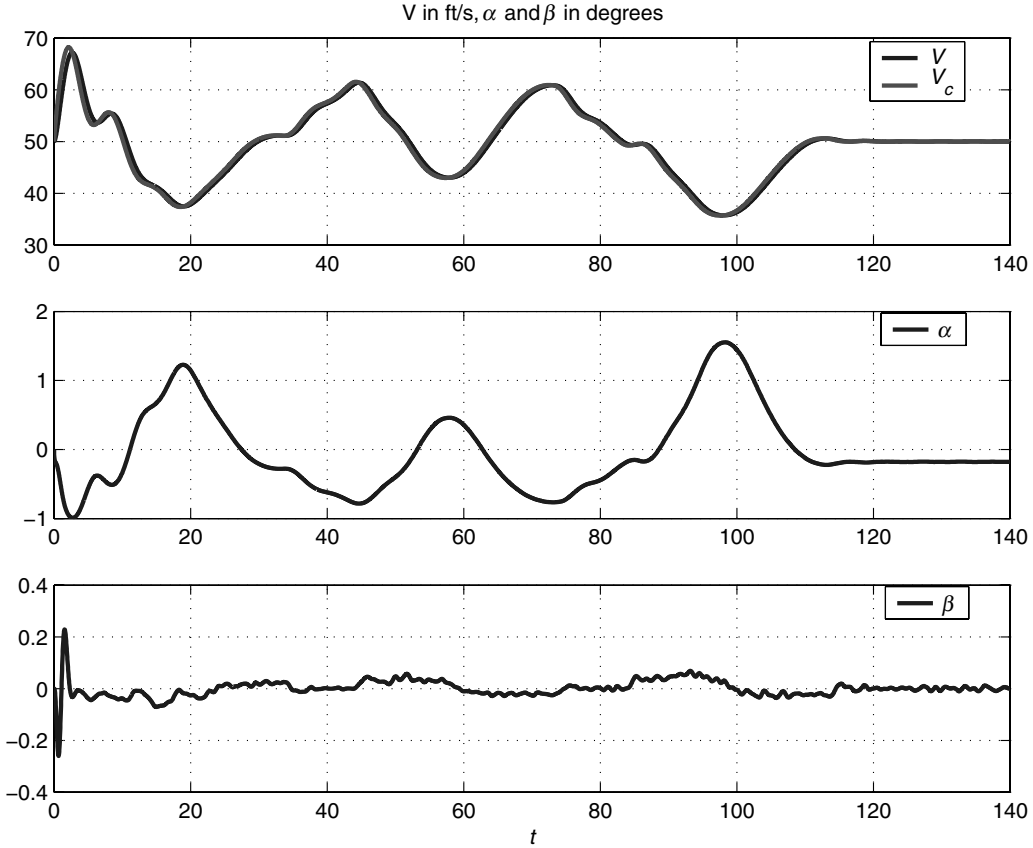


**Fig. 10 Wind frame velocity components.**

condition $\boldsymbol{r}(0)$. The desired inertial velocity is computed according to the guidance law in Eq. (55) along with the adaptive laws in Eq. (60), where the state estimate $\hat{\boldsymbol{r}}(t)$ is used, which is computed according to dynamics in Eq. (54). The airspeed command is computed according to Eq. (76) and the attitude angle commands are computed according to Eqs. (87–89).

Figure 4 shows that the guidance law is able to capture, after a short transient, the target's velocity profile with a small lag, which disappears when the target maintains a constant velocity. The parameter convergence is shown in Fig. 5. The target's size estimation gradually converges to the true value. The system output tracking is demonstrated in Fig. 6. The large discrepancy in $y$ and $z$ directions are due to the target's turning maneuvers in the horizontal plane and in the vertical direction. The resulting deflection commands are displayed in Fig. 7. The overall responses to the commands are represented in Figs. 8 and 9. The angles of attack and sideslip are in the acceptable range although are not controlled directly (Fig. 10). The angular rates have a good response after a small initial transient. The initial transient in all variables is due to a large initial relative separation compared with the reference command.

## VIII. Conclusions

An adaptive control framework that rejects time-varying disturbances is proposed to solve the tracking problem of a maneuvering target using only visual measurement. Although no direct measurement of the relative range is available, it is shown that the measurements of the image length and image centroid coordinates, obtained through the visual sensor, enable the follower to maintain the desired relative position with respect to the target in the presence of measurement noise, provided that the reference command has an additive intelligent excitation signal. It is shown that the latter is not required for the target interception problem. The methodology is limited to target maneuvers with a velocity that can be decomposed into a constant plus an $\mathcal{L}_\infty \bigcap \mathcal{L}_2$ term.

## Appendix: Projection Operator

The projection operator introduced in [23] ensures boundedness of the parameter estimates by definition. We recall the main definition from [23].

*Definition 1.* Consider a convex compact set with a smooth boundary given by

$$\Omega_c \triangleq \{\boldsymbol{\theta} \in \mathbb{R}^n \mid f(\boldsymbol{\theta}) \leq c\}, \qquad 0 \leq c \leq 1 \tag{A1}$$

where $f\colon \mathbb{R}^n \to \mathbb{R}$ is the following smooth convex function:

$$f(\boldsymbol{\theta}) = \frac{\boldsymbol{\theta}^\top \boldsymbol{\theta} - \theta_{\max}^2}{\epsilon_\theta} \tag{A2}$$

where $\theta_{\max} > 0$ is the norm bound imposed on the parameter vector $\boldsymbol{\theta}$, and $0 < \epsilon_\theta < 1$ denotes the convergence tolerance of our choice. For any given $\boldsymbol{y} \in \mathbb{R}^n$, the projection operator is defined as

$$\text{Proj}\,(\boldsymbol{\theta}, \boldsymbol{y}) = \begin{cases} \boldsymbol{y} & \text{if } f(\boldsymbol{\theta}) < 0 \\ \boldsymbol{y} & \text{if } f(\theta) \geq 0, \nabla f^\top \boldsymbol{y} \leq 0 \\ \boldsymbol{y} - \boldsymbol{g}(f, \boldsymbol{y}) & \text{if } f(\theta) \geq 0, \nabla f^\top \boldsymbol{y} > 0 \end{cases}$$

where

$$\boldsymbol{g}\,(f, \boldsymbol{y}) = \frac{\nabla f \nabla f^\top \boldsymbol{y}}{\|\nabla f\|^2} f(\boldsymbol{\theta}) \tag{A3}$$

□

The properties of the projection operator are given by the following lemma:

*Lemma 5.* Let $\boldsymbol{\theta}^* \in \Omega_0 = \{\boldsymbol{\theta} \in \mathbb{R}^n \mid f(\boldsymbol{\theta}) \leq 0\}$, and let the parameter $\theta(t)$ evolve according to the following dynamics:

$$\dot{\boldsymbol{\theta}}(t) = \text{Proj}(\boldsymbol{\theta}(t), \boldsymbol{y}), \qquad \boldsymbol{\theta}(t_0) \in \Omega_c \tag{A4}$$

Then,

$$\boldsymbol{\theta}\,(t) \in \Omega_c \tag{A5}$$

for all $t \geq t_0$, and

$$h_{\theta,y} \triangleq [\boldsymbol{\theta}(t) - \boldsymbol{\theta}^*]^\top [\mathrm{Proj}(\boldsymbol{\theta}(t), \boldsymbol{y}) - \boldsymbol{y}] \le 0 \tag{A6}$$

From Definition 1, it follows that $\boldsymbol{y}$ is not altered if $\boldsymbol{\theta}$ belongs to the set $\Omega_0$. In the set $\{0 \le f(\boldsymbol{\theta}) \le 1\}$, $\mathrm{Proj}(\boldsymbol{\theta}, \boldsymbol{y})$ subtracts a vector normal to the boundary of $\Omega_c$ so that we get a smooth transformation from the original vector field $\boldsymbol{y}$ to an inward or tangent vector field for $c = 1$. Therefore, on the boundary of $\Omega_c$, $\dot{\boldsymbol{\theta}}(t)$ always points toward the inside of $\Omega_c$ and $\boldsymbol{\theta}(t)$ never leaves the set $\Omega_c$, which is the first property.

From the convexity of function $f(\boldsymbol{\theta})$, it follows that for any $\boldsymbol{\theta}^* \in \Omega_0$ and $\boldsymbol{\theta} \in \Omega_c$, the inequality $l_{\boldsymbol{\theta}} \triangleq (\boldsymbol{\theta} - \boldsymbol{\theta}^*)^\top \nabla f(\boldsymbol{\theta}) \le 0$ holds. Then, from Definition 1 it follows that

$$h_{\theta,y} = \begin{cases} 0, & \text{if } f) < 0 \\ 0, & \text{if } f \ge 0,\ \nabla f^\top \boldsymbol{y} \le 0 \\ \dfrac{\underbrace{l_{\boldsymbol{\theta}}}_{\le 0}\ \underbrace{\nabla f^T \boldsymbol{y}}_{\ge 0}\ \underbrace{f(\boldsymbol{\theta})}_{\ge 0}}{\|\nabla f\|^2}, & \text{if } f \ge 0,\ \nabla f^\top \boldsymbol{y} > 0 \end{cases}$$

The second property follows.

The function $f_{\boldsymbol{d}}(\hat{\boldsymbol{d}})$ in the adaptive laws for the estimate $\hat{\boldsymbol{d}}(t)$ is defined as usual by

$$f_{\boldsymbol{d}}(\hat{\boldsymbol{d}}) = \frac{\hat{\boldsymbol{d}}^\top \hat{\boldsymbol{d}} - d_*^2}{\epsilon_d} \tag{A7}$$

From Lemma 5, it follows that the adaptive laws in Eqs. (17) and (60) guarantee the following inequalities:

$$\begin{gathered} \|\hat{\boldsymbol{d}}(t)\| \le d_* \\ \tilde{\boldsymbol{d}}^\top(t)[\mathrm{Proj}(\hat{\boldsymbol{d}}(t), \boldsymbol{e}(t)) - \boldsymbol{e}(t)] \le 0 \\ \tilde{\boldsymbol{d}}^\top(t)[\mathrm{Proj}(\hat{\boldsymbol{d}}(t), B_a^\top P_a \boldsymbol{\xi}_a^*(t)) - B_a^\top P_a \boldsymbol{\xi}_a^*(t)] \le 0 \end{gathered} \tag{A8}$$

provided that $\hat{\boldsymbol{d}}(0) \in \Omega_{\boldsymbol{d}}^0$.

We can impose some conservative lower and upper bounds on the parameter $b_T$ in the following form: $0 < b_{\min} \le b_T \le b_{\max}$. Therefore, the function $f_b(\hat{b})$ in the adaptive law for the estimate $\hat{b}$ can be defined as

$$f_b(\hat{b}) = \frac{[\hat{b} - (b_{\max} + b_{\min})/2]^2 - [(b_{\max} - b_{\min})/2]^2}{\epsilon_b} \tag{A9}$$

where $\epsilon_b$ denotes the convergence tolerance of our choice. According to Lemma 5 it follows that the adaptive laws in Eqs. (17) and (60) guarantee the following inequalities:

$$\begin{gathered} b_{\min} \le \hat{b}(t) \le b_{\max} \\ \tilde{b}(t)[\mathrm{Proj}(\hat{b}(t), \boldsymbol{e}^\top(t)\boldsymbol{g}(t)) - \boldsymbol{e}^\top(t)\boldsymbol{g}(t)] \le 0 \\ \tilde{b}(t)[\mathrm{Proj}(\hat{b}(t), \boldsymbol{g}(t)^\top B_a^\top P_a \boldsymbol{\xi}_a^*(t)) - \boldsymbol{g}(t)^\top B_a^\top P_a \boldsymbol{\xi}_a^*(t)] \le 0 \end{gathered} \tag{A10}$$

provided that $\hat{b}(0) \in \Omega_b^0$.

## Acknowledgments

Research for this paper was supported by the United States Air Force Office of Scientific Research under Multidisciplinary University Research Initiative subcontract F49620-03-1-0401. The authors are thankful to Anthony Calise, Chengyu Cao, and Vijay Patel for several stimulating and fruitful discussions.

## References

[1] Gurfil, P., and Kasdin, N. J., "Optimal Passive and Active Tracking Using the Two-Step Estimator," AIAA Paper 2002-5022, 2002.

[2] Weiss, H., and Moore, J. B., "Improved Extended Kalman Filter Design for Passive Tracking," *IEEE Transactions on Automatic Control*, Vol. AC-25, No. 4, 1980, pp. 807–811.

[3] Aidala, V. J., and Hammel, S. E., "Utilization of Modified Polar Coordinates for Bearings-Only Tracking," *IEEE Transactions on Automatic Control*, Vol. 28, No. 3, 1983, pp. 283–294.

[4] Balakrishnan, S. N., "Extension of Modified Polar Coordinates and Application with Passive Measurements," *Journal of Guidance, Control, and Dynamics*, Vol. 12, No. 6, 1989, pp. 906–912.

[5] Stallard, D. V., "Angle-Only Tracking Filter in Modified Spherical Coordinates," *Journal of Guidance, Control, and Dynamics*, Vol. 14, No. 3, 1991, pp. 694–696.

[6] Hepner, S. A. R., and Geering, H. P., "Adaptive Two Time-Scale Tracking Filter for Target Acceleration Estimation," *Journal of Guidance, Control, and Dynamics*, Vol. 14, No. 3, May–June 1991, pp. 581–588.

[7] Chang, W. T., and Lin, S. A., "Incremental Maneuver Estimation Model for Target Tracking," *IEEE Transactions on Aerospace and Electronic Systems*, Vol. 28, No. 2, April 1992, pp. 439–451.

[8] Oshman, Y., and Shinar, J., "Using a Multiple Model Adaptive Estimator in a Random Evasion Missile/Aircraft Estimation," AIAA Paper 99-4141, 1999.

[9] Bar-Shalom, Y., and Li, X. R., *Estimation and Tracking: Principles, Techniques and Software*, Artechhouse, Norwood, MA, 1993.

[10] Ljung, L., "Asymptotic Behavior of the Extended Kalman Filter as a Parameter Estimator for Linear Systems, *IEEE Transactions on Automatic Control*, Vol. 24, No. 1, 1979, pp. 36–50.

[11] Betser, A., Vela, P., and Tannenbaum, A., "Automatic Tracking of Flying Vehicles Using Geodesic Snakes and Kalman Filtering," *Proceedings of the 43rd IEEE Conference on Decision and Control*, Vol. 2, Inst. of Electrical and Electronics Engineers, 2004, pp. 1649–1654.

[12] Cao, C., and Hovakimyan, N., "Vision-Based Air-to-Air Tracking Using Intelligent Excitation," *Proceedings of the American Control Conference*, Vol. 7, American Automatic Control Council, 2005, pp. 5091–5096.

[13] Ke, Q., Kanade, T., Prazenica, R., and Kurdila, A., "Vision-Based Kalman Filtering for Aircraft State Estimation and Structure from Motion," AIAA Paper 2005-6003, 2005.

[14] Webb, T., Prazenica, R., Kurdila, A., and Lind, R., "Vision-Based State Estimation for Uninhabited Aerial Vehicles," AIAA Paper 2005-5869, 2005.

[15] Watkins, A., Prazenica, R., Kurdila, A., and Wiens, G., "RHC for Vision-Based Navigation of a WMR in an Urban Environment," AIAA Paper 2005-6094, 2005.

[16] Binev, P., Cohen, A., Dahmen, W., DeVore, R., and Temlyakov, V., "Universal Algorithms for Learning Theory Part 1 : Piecewise Constant Functions," *Journal of Machine Learning Research*, Vol. 6, Sept. 2005, pp. 1297–1321.

[17] Watanabe, Y., Johnson, E. N., and Calise, A. J., "Optimal 3-D Guidance from a 2-D Vision Sensor," AIAA Paper 2004-4779, 2004.

[18] Sattigeri, R., Calise, A. J., and Evers, J., "Adaptive Vision-Based Approach to Decentralized Formation Control," AIAA Paper 2004-5252, 2004.

[19] Sattigeri, R., Calise, A. J., and Evers, J. H., "Adaptive Approach to the Vision Based Formation Control," AIAA Paper 2003-5727, 2003.

[20] Marino, R., and Tomei, P., "Adaptive Tracking of Linear Systems with Arbitrarily Time-Varying Parameters," *Proceedings of the 38th IEEE Conference on Decision and Control*, Vol. 5, Inst. of Electrical and Electronics Engineers, 1999, pp. 5200–5205.

[21] Etkin, B., and Reid, L. D., *Dynamics of Flight: Stability and Control*, Wiley, New York, 1996.

[22] Sastry, S. S., and Bodson, M., *Adaptive Control: Stability, Convergence and Robustness*, Prentice–Hall, Upper Saddle River, NJ, 1989.

[23] Pomet, J. B., and Praly, L., "Adaptive Nonlinear Regulation: Estimation from the Lyapunov Equation," *IEEE Transactions on Automatic Control*, Vol. 37, No. 6, 1992, pp. 729–740.

[24] Marino, R., Santosuosso, G. L., and Tomei, P., "Robust Adaptive Observer for Nonlinear Systems with Bounded Disturbances," *IEEE Transactions on Automatic Control*, Vol. 46, No. 6, 2001, pp. 967–972.

[25] Slotine, J. J., and Li, W., *Applied Nonlinear Control*, Prentice–Hall, Upper Saddle River, NJ, 1991.

[26] Burl, J. B., *Linear Optimal Control: $\mathcal{H}_2$ and $\mathcal{H}_\infty$ Methods*, Addison–Wesley, Reading, MA, 1999.

[27] Bar-Shalom, Y., and Fortmann, T., *Tracking and Data Association*, Academic Press, London, 1988.

[28] Munro, B., "Airplane Trajectory Expansion for Dynamics Inversion," M.S. Thesis, Aerospace and Ocean Engineering Dept., Virginia Polytechnic Inst. and State Univ., Blacksburg, VA, 1992.

[29] Stevens, B. L., and Lewis, F. L., *Aircraft Control and Simulation*, Wiley, New York, 1992.

[30] Park, J., and Sandberg, I., "Universal Approximation Using Radial Basis Function Networks," *Neural Computation*, Vol. 3, 1991, pp. 246–257.

[31] Krstic, M., Kanellakopoulos, I., and Kokotovic, P., *Nonlinear and Adaptive Control Design*, Wiley, New York, 1995.